HHS Public Access

Author manuscript

Neuron. Author manuscript; available in PMC 2020 October 22.

Published in final edited form as:

Neuron. 2020 January 08; 105(1): 150–164.e6. doi:10.1016/j.neuron.2019.10.013.

Disruption of Oligodendrogenesis Impairs Memory Consolidation in Adult Mice

Patrick E. Steadman[1,2], **Frances Xia**[1,3], **Moriam Ahmed**[1], **Andrew J. Mocle**[1,3], **Amber R.A. Penning**[1], **Anna C. Geraghty**[4], **Hendrik W. Steenland**[1,5], **Michelle Monje**[4], **Sheena A. Josselyn**[1,2,3,6,7], **Paul W. Frankland**[1,2,3,6,8,9,*]

[1]Program in Neurosciences and Mental Health, Hospital for Sick Children, 555 University Avenue, Toronto, ON M5G 1X8, Canada

[2]Institute of Medical Sciences, University of Toronto, Toronto, ON M5S 1A8, Canada

[3]Department of Physiology, University of Toronto, Toronto, ON M5G 1X8, Canada

[4]Department of Neurology, Stanford University, Stanford, CA 94305, USA

[5]Max Planck Institute of Microstructure Physics, Halle 06120, Germany

[6]Department of Psychology, University of Toronto, Toronto, ON M5S 3G3, Canada

[7]Brain, Mind and Consciousness Program, Canadian Institute for Advanced Research, Toronto, ON M5G 1M1, Canada

[8]Child and Brain Development Program, Canadian Institute for Advanced Research, Toronto, ON M5G 1M1, Canada

[9]Lead Contact

SUMMARY

The generation of myelin-forming oligodendrocytes persists throughout life and is regulated by neural activity. Here we tested whether experience-driven changes in oligodendrogenesis are important for memory consolidation. We found that water maze learning promotes oligodendrogenesis and *de novo* myelination in the cortex and associated white matter tracts. Preventing these learning-induced increases in oligodendrogenesis without affecting existing oligodendrocytes impaired memory consolidation of water maze, as well as contextual fear, memories. These results suggest that *de novo* myelination tunes activated circuits, promoting coordinated activity that is important for memory consolidation. Consistent with this, contextual fear learning increased the coupling of hippocampal sharp wave ripples and cortical spindles, and

*Correspondence: paul.frankland@sickkids.ca.

AUTHOR CONTRIBUTIONS

Conception, P.E.S. and P.W.F.; Methodology, P.E.S. and P.W.F.; Investigation, P.E.S., M.A., A.R.A.P., A.C.G., A.J.M., F.X., and H.W.S.; Writing – Original Draft, P.E.S., S.A.J., and P.W.F.; Writing – Review & Editing, P.W.F., P.E.S., F.X., S.A.J., and M.M.; Funding Acquisition, P.W.F. and S.A.J.

SUPPLEMENTAL INFORMATION

Supplemental Information can be found online at https://doi.org/10.1016/j.neuron.2019.10.013.

DECLARATION OF INTERESTS

The authors declare no competing interests.

these learning-induced increases in ripple-spindle coupling were blocked when oligodendrogenesis was suppressed. Our results identify a non-neuronal form of plasticity that remodels hippocampal-cortical networks following learning and is required for memory consolidation.

Graphical Abstract

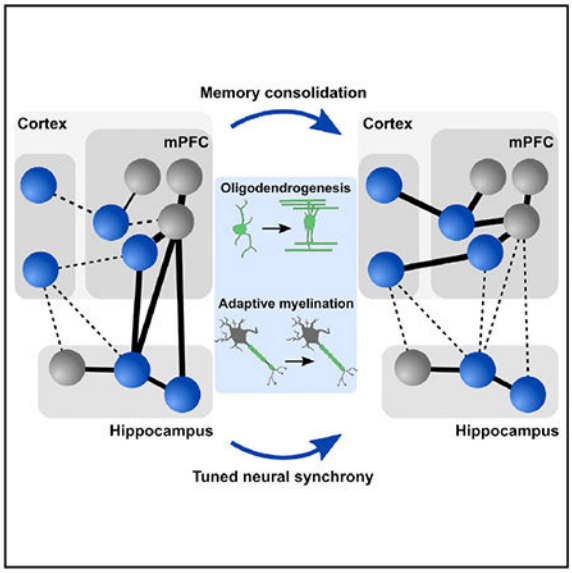

In Brief

Experience-dependent *de novo* myelination may fine-tune activated circuits by promoting brain synchrony, important for memory consolidation. Steadman et al. find that blocking this form of adaptive myelination prevents learning-induced increases in coordinated activity and impairs memory consolidation.

INTRODUCTION

Animals may learn to associate places with either appetitive stimuli (e.g., food) or aversive stimuli (e.g., a predator). This form of spatial learning broadly engages cortical and hippocampal neural circuits, and successful consolidation of spatial memories is thought to lead to enduring modifications of these neural circuits. To date, learning-induced modifications have mostly been studied at the level of the synapse and at the time of encoding, with changes in synaptic strength in the hippocampus shown to contribute critically to spatial memory formation (Takeuchi et al., 2013). However, the speed of conduction of signals along axons may also affect neural circuit plasticity. Modifications that promote synchrony of spike timing arrival or oscillator coupling may contribute to the efficiency of memory encoding and to the subsequent consolidation of those memories at later stages (Pajevic et al., 2014).

Neuronal conduction speed along an axon depends on the axon diameter together with the thickness and spacing of myelin. Oligodendrocyte precursor cells (OPCs) represent the

largest population of dividing cells in the adult brain and generate myelin-forming oligodendrocytes throughout life (Hill et al., 2018; Hughes et al., 2013; Kang et al., 2010). Because OPC proliferation and differentiation into myelin-forming oligodendrocytes is regulated by neural activity (Gibson et al., 2014; Hughes et al., 2018; Mitew et al., 2018; Wake et al., 2011), this raises the possibility that adult oligodendrogenesis and associated changes in myelin patterning may dynamically remodel activated circuits in an experience-dependent manner. In the adult cortex, there is a large degree of variance in myelin patterning in cortical axons and, therefore, potential for experience-dependent myelin remodeling (Hughes et al., 2018; Tomassy et al., 2014). Such myelin remodeling likely contributes to memory encoding (Geraghty et al., 2019; McKenzie et al., 2014; Xiao et al., 2016). However, this form of plasticity may also be important during post-encoding "offline" periods, when coupling of rhythmic oscillations in hippocampal-cortical networks is thought to be necessary for successful consolidation of spatial memory (Buzsáki, 1996; Diekelmann and Born, 2010). In particular, coupling of cortical spindle oscillations and hippocampal sharp wave ripples is important for memory consolidation (Peyrache et al., 2009, 2011; Siapas and Wilson, 1998). Interventions that promote ripple-spindle coupling facilitate memory consolidation (Maingret et al., 2016). Conversely, interventions that decouple these oscillations impair consolidation (Xia et al., 2017). These results suggest that small perturbations in timing may desynchronize the timing of spikes arriving at key synapses and thereby decouple these oscillators.

Here we provide four lines of evidence that support this hypothesis. First, we find that oligodendrogenesis and *de novo* myelination formation is increased following spatial learning in the water maze. Increased oligodendrogenesis was observed in cortical gray and white matter regions associated with spatial memory consolidation and occurred both during training, as well as immediately following training. Second, inhibition of oligodendrogenesis (without affecting existing myelin patterns), either during learning or immediately following learning, impaired consolidation of spatial memory. Third, inhibition of oligodendrogenesis similarly impaired consolidation of contextual fear memory, another form of learning that engages hippocampal-cortical circuits. Fourth, contextual fear conditioning led to increases in coupling of hippocampal ripples and cortical spindles. Inhibition of oligodendrogenesis prevented this learning-induced increase in oscillatory coupling and impaired contextual fear memory consolidation in the same mice. These results suggest that adult oligodendrogenesis plays a critical and previously unappreciated role in memory consolidation, most likely via fine-tuning myelin patterns to promote hippocampal-cortical communication following learning.

RESULTS

Deletion of the Transcription Factor Mrf from OPCs Disrupts Adult Oligodendrogenesis in the Cerebral Cortex and *Corpus Callosum*

To test the hypothesis that the formation of new myelinating oligodendrocytes is necessary for memory consolidation, we used mice in which administration of the synthetic ligand tamoxifen (TAM) or its metabolite 4-hydroxy-TAM (4OHT) induces expression of the fluorescent protein TdTomato (TdT) and deletes myelin regulatory factor (Mrf) from OPCs

(NG2-cre^{ERTM} × Mrf$^{fl/fl}$ × Ai14 or Mrf$_{CKO}$ mice). Mrf is a transcription factor that is required for oligodendrocytes to initiate and maintain their myelination program, and its loss in OPCs prevents maturation of adult-generated oligodendrocytes without affecting existing oligodendrocytes (Figure 1A; Emery et al., 2009; McKenzie et al., 2014; Xiao et al., 2016). NG2-cre^{ERTM} × Ai14 (Mrf$_{CON}$) mice were used as controls.

To assess the effects of Mrf deletion in OPCs on oligodendrogenesis, young adult (i.e., 10-week-old) Mrf$_{CKO}$ and Mrf$_{CON}$ mice were treated with 4OHT, and tissue from the retrosplenial cortex and *corpus callosum* was evaluated 4 days later (Figures 1B and 1C). In Mrf$_{CON}$ mice, approximately 70% of OPCs were TdT$^+$ (i.e., TdT$^+$|Olig2$^+$/PDGFRα$^+$) (Figures S1A and S1B), reflecting efficient recombination in OPC cells, as observed previously using this TAM-inducible cre driver line (Rivers et al., 2008). Moreover, in Mrf$_{CON}$ mice, ~74% of TdT$^+$ cells expressed Olig2 (i.e., Olig2$^+$|TdT$^+$) (Figure S1C), indicating that recombination is largely restricted to oligodendrocyte lineage cells. In these same regions, recombination in non-oligodendrocyte lineage cells was low or negligible (Figures S1D–S1F).

As expected, Mrf deletion in OPCs reduced adult oligodendrogenesis. In the retrosplenial cortex, the numbers of TdT$^+$ and TdT$^+$/Olig2$^+$ cells were reduced in Mrf$_{CKO}$ mice compared with Mrf$_{CON}$ mice following 4OHT treatment (t_{13} = 2.29, p = 0.040) (Figure 1D; Figures S1G and S1H). Importantly, the numbers of TdT$^-$/Olig2$^+$ cells did not change (t_{13} = 0.42, p = 0.68) (Figure 1E), indicating that Mrf deletion in OPCs only affected adult oligodendrogenesis and did not affect existing oligodendrocytes. Reduced adult oligodendrogenesis was driven by loss of adult-generated oligodendrocytes rather than OPCs. In 4OHT-treated Mrf$_{CKO}$ mice, there were fewer adult-generated oligodendrocytes (i.e., TdT$^+$/Olig2$^+$/CC1$^+$ cells; t_8 = 4.13, p = 0.0033) (Figure 1F), but the numbers of OPCs (i.e., TdT$^+$/Olig2$^+$/PDGFRα$^+$ cells) were similar in both groups (Figures S1G–S1I). 4OHT-treatment similarly attenuated adult oligodendrogenesis in the *corpus callosum* (Figure S1J), indicating that Mrf deletion reduced adult oligodendrogenesis in both white and gray matter regions.

Reduced adult oligodendrogenesis was evident within 4 days of Mrf deletion. We next assessed whether this reduction persisted. Adult Mrf$_{CKO}$ and Mrf$_{CON}$ mice were treated with TAM and were perfused 4 weeks later (Figure 1G). We assessed adult oligodendrogenesis in the retrosplenial cortex, *alveus*, and *corpus callosum/cingulum.* Four weeks following Mrf inactivation, reduced adult oligodendrogenesis (i.e., TdT$^+$ or TdT$^+$/Olig2$^+$ cells) was observed in the retrosplenial cortex, *corpus callosum/cingulum*, and *alveus*. This reduction was driven by loss of adult-generated oligodendrocytes (i.e., TdT$^+$/Olig2$^+$/CC1$^+$ cells: *alveus*, t_4 = 4.44, p = 0.011; *corpus callosum/cingulum*, t_4 = 2.93, p = 0.043; retrosplenial cortex, t_4 = 3.60, p = 0.023) (Figures 1H–1M) rather than OPCs (i.e., TdT$^+$/Olig2$^+$/PDGFRα$^+$ cells) (Figures S1K–S1N).

Spatial Learning Induces Adult Oligodendrogenesis

Spatial learning engages hippocampal-cortical networks (Teixeira et al., 2006). Because neural activity induces oligodendrogenesis (Barres and Raff, 1993; Demerens et al., 1996;

Gibson et al., 2014; Hughes et al., 2018; McKenzie et al., 2014; Mitew et al., 2018), we next evaluated whether oligodendrogenesis occurs within these circuits during learning.

Wild-type (WT) mice were trained to locate a fixed platform (4 days, 3 trials per day) in the water maze. Spatial memory was then assessed in a probe test 1 day following training, with the platform removed from the pool. To assess proliferation of oligodendrocyte lineage cells during the training period, mice were administered the thymidine analog 5-ethynyl-2′-deoxyuri-dine (EdU) throughout training via their drinking water (i.e., a labeling period of 96 h). The number and phenotype of EdU^+ cells were assessed immediately following completion of the probe test in hippocampal and cortical regions (Figure 2A).

Over the course of training, mice found the platform with decreasing latency (one-way repeated-measures ANOVA; $F_{1,26} = 28.72$, $p < 0.0001$) (Figure 2B). In the probe test, compared with either non-trained controls (CON) or time-yoked swimming controls (SWM), trained (TRN) mice searched selectively in the region of the pool that formerly contained the platform (two-way repeated-measures ANOVA: condition [$F_{2,30} = 22.68$, $p < 0.0001$], zone [$F_{2,30} = 2.50$, $p = 0.12$], condition × zone interaction [$F_{2,30} = 18.16$, $p < 0.0001$]; for target zone, TRN > CON and TRN > SWM by Tukey [HSD] post hoc test) (Figure 2C).

Analysis of EdU^+ cells revealed that adult oligodendrogenesis increased during training (compared with CON/SWM mice) in some but not all brain regions analyzed (anterior cingulate cortex, $F_{2,12} = 0.59$, $p = 0.57$; prelimbic/infralimbic cortex, $F_{2,12} = 3.05$, $p = 0.076$; retrosplenial cortex, $F_{2,12} = 4.23$, $p = 0.032$ [TRN > CON and TRN > SWM by Tukey HSD post hoc test]; CA1 region of the hippocampus, $F_{2,12} = 0.78$, $p = 0.48$) (Figure 2D). These increases were primarily driven by an increase in the number of adult-generated oligodendrocytes (i.e., $EdU^+/Olig2^+/CC1^+$ cells: anterior cingulate cortex, $F_{2,12} = 14.88$, $p = 0.00056$ [TRN > CON and TRN > SWM by Tukey HSD post hoc test]; prelimbic/infralimbic cortex, $F_{2,12} = 1.27$, $p = 0.31$; retrosplenial cortex, $F_{2,12} = 6.39$, $p = 0.0085$ [TRN > CON and TRN > SWM by Tukey HSD post hoc test]; CA1 region of the hippocampus, $F_{2,12} = 1.56$, $p = 0.25$) (Figure 2E). In addition, the OPC pool (i.e., $EdU_+/Olig2_+/PDGFR\alpha_+$ cells) expanded in the retrosplenial cortex but not in other regions (Figures S2A and S2B).

Disrupting Oligodendrogenesis Impairs Spatial Learning

We next tested whether preventing training-induced increases in adult oligodendrogenesis would impair spatial learning. To do this, we crossed NG2-cre^{ERTM} × $Mrf^{fl/fl}$ mice and trained their cre+ (Mrf_{CKO} mice) and cre− (Mrf_{CON} mice) offspring in the water maze. During training, mice were treated with 4OHT, and spatial memory was tested in a probe test 1 day following completion of training (Figure 2F). Across training days, mice required progressively less time to locate the platform, indicating robust learning, and there were no differences between genotypes (genotype [$F_{1,22} = 0.02$, $p = 0.89$], training [$F_{1,70} = 77.44$, $p < 0.0001$], genotype × training interaction [$F_{1,70} = 1.53$, $p = 0.22$]) (Figure 2G). However, in the probe test, Mrf_{CKO} mice searched less selectively than Mrf_{CON} mice (genotype [$F_{1,22} = 4.36$, $p = 0.049$], zone [$F_{1,22} = 96.90$, $p < 0.0001$], genotype × zone interaction [$F_{1,22} = 9.02$, $p = 0.0065$]) (Figures 2H and 2I). Although both Mrf_{CON} and Mrf_{CKO} mice spent more time

searching the target versus non-target zones, time spent in the target zone was reduced in Mrf_{CKO} mice (p = 0.00038, Tukey HSD post hoc test). Importantly, swim speed was similar in Mrf_{CKO} and Mrf_{CON} mice in the probe test (t_{22} = 0.95, p = 0.35) (Figure 2J), suggesting that Mrf deletion did not produce general motor impairments.

Previous studies have shown that motor learning (McKenzie et al., 2014; Xiao et al., 2016) and sensory enrichment (Hughes et al., 2018) induce oligodendrogenesis in motor and somatosensory cortices, respectively. Furthermore, suppressing oligodendrogenesis impairs motor learning (McKenzie et al., 2014). The current findings indicate that spatial learning induces similar changes in integrative cortical regions (e.g., the anterior cingulate and retrosplenial cortices). Moreover, our data suggest that these experience-driven changes in oligodendrogenesis are necessary for spatial learning.

Spatial Memory Consolidation Induces Adult Oligodendrogenesis

Successful memory consolidation requires continued neural processing following training (Carr et al., 2011). In the previous experiments, training took place over several days. Therefore, oligodendrogenesis might be induced either by neural activity during training or by neural activity that occurs in periods between daily training sessions. We next evaluated whether oligodendrogenesis occurs during the post-training consolidation period, in the absence of any additional training.

WT mice were trained to locate a fixed platform (6 days, 3 trials per day) in the water maze. Spatial memory was then assessed in probe tests 1 day (recent) and 28 days (remote) following training. To assess proliferation of oligodendrocyte-lineage cells during the post-training period, mice were administered EdU (for 4 days), starting immediately following training. The number and phenotype of EdU^+ cells were assessed immediately following completion of the second (remote) probe test in hippocampal, cortical, and associated white matter regions (Figure 3A).

Over the course of training, mice found the platform with decreasing latency (one-way repeated-measures ANOVA; $F_{1,39}$ = 42.74, p < 0.0001) (Figure 3B). In the probe tests, compared with controls (CON, SWM), TRN mice searched selectively in the region of the pool that formerly contained the platform, and their performance did not decrease with time (recent probe, two-way repeated-measures ANOVA: condition [$F_{2,23}$ = 12.36, p = 0.0002], zone [$F_{1,23}$ = 4.74, p = 0.040], condition × zone interaction [$F_{2,23}$ = 11.63, p = 0.0003], for target zone, TRN > CON and TRN > SWM by Tukey HSD post hoc test; remote probe, two-way repeated-measures ANOVA: condition [$F_{2,23}$ = 27.55, p < 0.0001], zone [$F_{1,23}$ = 29.82, p < 0.0001], condition × zone interaction [$F_{2,23}$ = 18.99, p < 0.0001], for target zone, TRN > CON and TRN > SWM by Tukey HSD post hoc test) (Figures 3C and 3D).

Analysis of EdU^+ cells revealed that adult oligodendrogenesis increased following training (compared with CON and SWM mice) in some but not all brain regions analyzed (anterior cingulate cortex, $F_{2,14}$ = 9.16, p = 0.0029 [TRN > CON and TRN > SWM by Tukey HSD post hoc test]; prelimbic/infralimbic cortex, $F_{2,15}$ = 12.62, p = 0.00061 [TRN > CON and TRN > SWM by Tukey HSD post hoc test]; retrosplenial cortex, $F_{2,15}$ = 3.40, p = 0.061; CA1 region of the hippocampus, $F_{2,16}$ = 1.49, p = 0.26; *alveus*, $F_{2,14}$ = 0.45, p = 0.64;

corpus callosum/cingulum, $F_{2,14}$ = 7.23, p = 0.0070 [TRN > CON and TRN > SWM by Tukey HSD post hoc test]). Furthermore, these increases were primarily driven by an increase in oligodendrocyte lineage cells (i.e., $EdU^+/Olig2^+$ cells), with increased numbers of adult-generated oligodendrocytes (i.e., $EdU^+/Olig2^+/CC1^+$ cells: anterior cingulate cortex, $F_{2,14}$ = 10.09, p = 0.0019 [TRN > CON and TRN > SWM by Tukey HSD post hoc test]; prelimbic/infralimbic cortex, $F_{2,15}$ = 11.21, p = 0.0011 [TRN > CON and TRN > SWM by Tukey HSD post hoc test]; retrosplenial cortex, $F_{2,15}$ = 1.00, p = 0.39; CA1 region of the hippocampus, $F_{2,16}$ = 0.38, p = 0.26; *alveus*, $F_{2,14}$ = 2.22, p = 0.15; *corpus callosum/cingulum*, $F_{2,14}$ = 19.85, p = 8.19×10^{-5} [TRN > CON and TRN > SWM by Tukey HSD post hoc test]) and an expanded OPC pool (i.e., $EdU^+/Olig2^+/PDGFR\alpha^+$ cells: anterior cingulate cortex, $F_{2,14}$ = 0.03, p = 0.97; prelimbic/infralimbic cortex, $F_{2,13}$ = 3.66, p = 0.054 [TRN > CON by Tukey HSD post hoc test]; retrosplenial cortex, $F_{2,14}$ = 0.42, p = 0.67; CA1 region of the hippocampus, $F_{2,14}$ = 0.73, p = 0.50; *alveus*, $F_{2,14}$ = 0.38, p = 0.69; *corpus callosum/cingulum*, $F_{2,13}$ = 6.43, p = 0.011 [TRN > CON and TRN > SWM by Tukey HSD post hoc test]) (Figures 3E–3G; Figures S3A and S3B).

The increase in oligodendrocytes suggests that consolidation leads to *de novo* myelination. To test this, we used electron microscopy to examine myelin content following water maze training in the *corpus callosum/cingulum* and *alveus*. Training was associated with an increase in the number of myelinated axons (*alveus*, t_5 = 0.94, p = 0.38; *corpus callosum/cingulum*, t_4 = 3.99, p = 0.016) relative to non-trained controls (Figures 3H–3J). Importantly, these changes were limited to the same region (i.e., *corpus callosum/cingulum*) where we observed consolidation-associated oligodendrogenesis. In contrast, water maze training did not affect myelin thickness in either region, as measured by the g-ratio of myelinated axons (diameter of the axon divided by the diameter of the axon plus the myelin sheath; *alveus*, t_4 = 0.22, p = 0.84; *corpus callosum/cingulum*, t_4 = 0.16, p = 0.88) (Figures 3K and 3L). The absence of an effect on myelin thickness suggests that learning does not significantly affect existing myelin patterns. Instead, spatial learning induces addition of new myelin sheaths, consistent with recent reports showing experience-driven *de novo* myelination in adult mice (Hill et al., 2018; Hughes et al., 2018).

These findings indicate that adult oligodendrogenesis increases following spatial learning in the absence of additional training. Increases were observed in the prefrontal cortex (including the prelimbic, infralimbic, and anterior cingulate cortices) and the *corpus callosum/cingulum*. This raises the possibility that myelin remodeling in the post-training period is largely restricted to regions associated with long-term consolidation of spatial information (Kitamura et al., 2017; Takehara-Nishiuchi, 2014; Vetere et al., 2011, 2017), including water maze memories (Teixeira et al., 2006), rather than regions associated with initial encoding of spatial information (e.g., the CA1 region of the hippocampus).

Disrupting Oligodendrogenesis Impairs Consolidation of Spatial Learning

We next tested whether preventing training-induced increases in adult oligodendrogenesis would impair consolidation of spatial memories. Mrf_{CKO} and Mrf_{CON} mice were trained in the water maze and, following training, treated with TAM to delete Mrf in OPCs. Spatial memory was tested in probe tests 1 day (recent test) and 28 days (remote test) following

completion of training (Figure 4A). Across training days, mice required progressively less time to locate the platform, and there were no differences between genotypes (genotype [$F_{1,47}$ = 1.14, p = 0.29], training [$F_{1,243}$ = 295.16, p < 0.0001], genotype × training interaction [$F_{1,243}$ = 0.27, p = 0.60]) (Figure 4B). In the recent probe test, Mrf_{CKO} and Mrf_{CON} mice searched selectively. Both Mrf_{CKO} and Mrf_{CON} mice spent more time in the zone centered on the former platform location (compared with other, equivalent zones), and there was no difference in target zone dwelling time between genotypes (genotype [$F_{1,47}$ = 0.15, p = 0.70], zone [$F_{1,47}$ = 135.74, p < 0.0001], genotype × zone interaction [$F_{1,47}$ = 0.11, p = 0.74]) (Figures 4C and 4D).

In contrast, in the remote memory test, Mrf_{CKO} mice searched less selectively than Mrf_{CON} mice (genotype [$F_{1,47}$ = 3.33, p = 0.074], zone [$F_{1,47}$ = 63.36, p < 0.0001], genotype × Zone interaction [$F_{1,47}$ = 4.24, p = 0.045]) (Figures 4C and 4E; Figures S4A–S4D). Although both Mrf_{CON} and Mrf_{CKO} mice spent more time searching target versus non-target zones, the time spent in the target zone was reduced in Mrf_{CKO} mice (p = 0.0072, Tukey HSD post hoc test). Importantly, swim speed was similar in Mrf_{CKO} and Mrf_{CON} mice in both the recent (t_{47} = 0.056, p = 0.96) and remote (t_{47} = 0.43, p = 0.67) probe tests (Figures 4F and 4G), suggesting that Mrf deletion did not produce general motor impairments. Moreover, expression of the cre^{ERTM} transgene in OPCs did not affect maze learning or swim speed (Figures S4E–S4J). Because Mrf inactivation occurred after training was completed, these results indicate that adult oligodendrogenesis is required in this post-training period for successful consolidation of water maze memories.

To evaluate whether this finding would generalize across a range of experimental conditions, we performed additional control experiments. First, we used a second mouse line to drive expression of cre^{ERTM} in OPCs (PDGFRα-cre^{ERTM}) and crossed these mice with $Mrf^{fl/fl}$ mice. In adult offspring from this cross, Mrf inactivation following water maze training similarly impaired spatial memory consolidation, supporting the conclusion that post-training Mrf inactivation in OPCs, regardless of cre driver line, impairs spatial memory consolidation (Figures S4K–S4R).

Second, in the above experiments, spatial memory was assessed in consecutive, non-reinforced probe tests. Therefore, it is possible that less selective searching in Mrf_{CKO} mice at the remote time point might reflect accelerated extinction (rather than impaired consolidation). To address this potential confound, we trained Mrf_{CKO} and Mrf_{CON} mice as before but omitted the recent probe test. At the remote time point, Mrf_{CKO} mice again showed impaired memory, searching less selectively than Mrf_{CON} mice in the probe test (Figures S4S–S4U). These findings indicate that accelerated extinction cannot account for impaired performance of Mrf_{CKO} mice at the remote time point.

Disrupting Oligodendrogenesis Reduces Myelination and Impairs Spatial Memory Consolidation

We next confirmed that preventing training-induced changes in adult oligodendrogenesis impairs memory consolidation using a within-subject design. To do this, adult Mrf_{CKO} and Mrf_{CON} mice were trained in the water maze and co-administered TAM and EdU during the

immediate post-training period (Figure 5A). As previously, Mrf_{CKO} showed impaired spatial memory in the probe test 28 days following training (Figures S5A–S5D).

To assess oligodendrogenesis in the immediate post-training period, the number and phenotype of EdU^+ cells were assessed in hippocampal, cortical, and associated white matter regions following completion of the second (remote) probe test (Figure 5B; Figures S5E and S5F). Mrf inactivation reduced numbers of EdU^+ cells. This reduction reflected a decrease in oligodendrocyte-lineage cells and, in particular, a decrease in mature oligodendrocytes (i.e., $EdU^+/Olig2^+/CC1^+$ cells; anterior cingulate cortex, $t_{11} = 2.35$, p = 0.039; prelimbic/infralimbic cortex, $t_{12} = 2.32$, p = 0.039; *alveus*, $t_8 = 4.46$, p = 0.0021; *corpus callosum/cingulum*, $t_9 = 4.23$, p = 0.0022) (Figure 5C).

The reduction in mature oligodendrocytes following Mrf deletion predicts that there should be a reduction in myelinated axons within these regions. To test this, we examined myelin content in the *alveus* and *corpus callosum/cingulum* using electron microscopy in mice trained in the water maze (Figure 5D). We found that Mrf inactivation reduced the number of myelinated axons (*alveus*: $t_5 = 4.49$, p = 0.0065; *corpus callosum/cingulum*: $t_4 = 4.90$, p = 0.0080) (Figures 5E and 5F). In contrast, Mrf inactivation did not affect myelin thickness, as measured by the g-ratio of myelinated axons (*alveus*: $t_5 = 0.32$, p = 0.76; *corpus callosum/cingulum*: $t_5 = 1.55$, p = 0.18) (Figures 5G and 5H).

Disrupting Oligodendrogenesis at Remote Time Points Does Not Impair Spatial Memory

Interventions that disrupt activity and/or plasticity in the prefrontal cortex around the time of training (but not at more remote time points) impair subsequent memory expression (Kitamura et al., 2017; Takehara-Nishiuchi, 2014; Vetere et al., 2017; 2011). We therefore reasoned that Mrf inactivation in OPCs at more remote delays would be less likely to impair spatial memory. To test this, Mrf_{CKO} and their littermate controls were trained in the water maze. As previously, spatial memory was tested in probe tests 1 day and 28 days following the completion of training. However, in this experiment, TAM administration was delayed until 25 days following training rather than immediately following training (Figure 6A).

Across training days, mice required progressively less time to locate the platform, and there were no differences between genotypes (genotype [$F_{1,16} = 1.00$, p = 0.33], training [$F_{1,88} = 60.86$, p < 0.0001], genotype × training interaction [$F_{1,88} = 0.59$, p = 0.44]) (Figure 6B). In both recent and remote probe tests, Mrf_{CKO} and Mrf_{CON} mice searched selectively. At the recent time point, both Mrf_{CKO} and Mrf_{CON} mice spent more time in the zone centered on the former platform location (compared with other, equivalent zones), and there was no difference in target zone dwelling between genotypes (genotype [$F_{1,21} = 0.60$, p = 0.45], zone [$F_{1,21} = 39.82$, p <0.0001], genotype × zone interaction [$F_{1,21} = 0.29$, p = 0.60]) (Figures 6C and 6D). Similarly, at the remote memory time point, both Mrf_{CKO} and Mrf_{CON} mice spent more time in the zone centered on the former platform location (compared with other, equivalent zones), and there was no difference in target zone dwelling between genotypes (genotype [$F_{1,21} = 0.21$, p = 0.65], zone [$F_{1,21} = 24.87$, p = 0.0001], genotype × zone interaction [$F_{1,21} = 0.23$, p = 0.63]) (Figures 6C and 6E).

These data suggest that there is a specific post-training time window during which adaptive myelination contributes to memory consolidation. Furthermore, our observation of normal spatial memory when Mrf was deleted at remote time points indicates that Mrf inactivation in OPCs does not affect memory retrieval, nor does inhibiting adult oligodendrogenesis interfere non-specifically with the ability of mice to express a spatial memory (e.g., by impairing swimming). Consistent with this, swim speeds were equivalent in Mrf_{CKO} and Mrf_{CON} mice in probe tests (recent probe: $t_{21} = 0.36$, p = 0.73; remote probe: $t_{21} = 0.57$, p = 0.58) (Figures 6F and 6G; Figures S6A–S6D).

Reduced Oligodendrogenesis Impairs Learning-Induced Increases in Ripple-Spindle Coupling

Experience-induced oligodendrogenesis in the adult brain is hypothesized to be important for memory consolidation by coordinating neural activity across brain regions and, in particular, synchronizing rhythmic oscillations (Pajevic et al., 2014). Specifically, coupling between spindle oscillations in the prefrontal cortex and sharp wave ripple oscillations in the hippocampus is thought to contribute to memory consolidation (Siapas and Wilson, 1998). Learning leads to an increase in ripple-spindle coupling, and this increased oscillatory coupling appears to play an essential role in memory consolidation (Maingret et al., 2016; Xia et al.,2017).

To address this question, we used a contextual fear conditioning paradigm because this form of learning engages hippocampal-cortical circuits and, importantly, allows recording of neural activity prior to and immediately following training. We implanted local field potential electrodes in the prefrontal cortex (specifically, the anterior cingulate cortex [ACC]) and the hippocampus (specifically, the CA1 region of the dorsal hippocampus) in Mrf_{CON} and Mrf_{CKO} mice. Following recovery, mice were habituated to the recording chamber, and baseline recordings of neural activity were acquired. Following baseline recording, mice were treated with 4OHT and then fear conditioned. Neural activity was recorded immediately following training and contrasted with the pre-training baseline. Memory was assessed 28 days following training (Figure 7A).

We reliably detected spindles and ripples in the ACC and CA1, respectively, using previously established criteria (Boyce et al., 2016; Eschenko et al., 2006; Xia et al., 2017; Figure 7B). To evaluate the effect of Mrf inactivation on local activity, we assessed the density and amplitude of these oscillations during non-REM sleep. Neither training nor Mrf inactivation altered the density or amplitude of ripples (density, $t_9 = 1.36$, p = 0.21; amplitude $t_9 = 1.83$, p = 0.10) (Figures 7C and 7D; Figure S7B) or spindles (density $t_9 = 0.58$, p = 0.58; amplitude $t_9 = 0.62$, p = 0.55) (Figures 7E and 7F; Figure S7C).

To evaluate the effect of Mrf inactivation on coordinated activity between the ACC and CA1, we computed the cross-correlation between ripple and spindle amplitudes. In Mrf_{CON} mice, we observed a conditioning-dependent increase in this correlation, consistent with previous studies showing learning-induced increases in ripple-spindle coupling (Maingret et al., 2016; Xia et al., 2017). In contrast, Mrf deletion from OPCs prevented this learning-induced increase in coupling (Figures 7G and 7H). An ANOVA (with genotype as a between-subjects variable and recording session as a within-subject variable) supported these observations

(genotype [$F_{1,9}$ = 6.15, p = 0.035], session [$F_{1,9}$ = 1.05, p = 0.33], genotype × session interaction [$F_{1,9}$ = 11.19, p = 0.0086], p = 0.0052, Tukey HSD post hoc test of Mrf_{CON} for pre- versus post-training, p = 0.00046, Tukey HSD post hoc test of the post-training session for Mrf_{CON} versus Mrf_{CKO}) (Figure 7I; Figure S7D). An identical pattern was observed using ripple-spindle joint occurrence rate, a second metric of coupling (genotype [$F_{1,9}$ = 0.75, p = 0.41], session [$F_{1,9}$ = 0.88, p = 0.37], genotype × session interaction [$F_{1,9}$ = 8.06, p = 0.019], p = 0.037, Tukey HSD post hoc test of Mrf_{CON} for pre- versus post-training) (Figure 7J; Figure S7E). The lag between ripple and spindle peak amplitude was ~110 ms. This is consistent with previous studies and was not affected by training or by Mrf deletion (Figure S7F). Moreover, Mrf inactivation did not alter the proportion of non-REM sleep (Figure S7G), so changes in coupling cannot be attributed to changes in sleep architecture.

Critically, Mrf_{CKO} mice, in which learning-induced increases in ripple-spindle coupling were disrupted, exhibited reduced freezing when tested 28 days following training (t_9 = 3.73, p = 0.0047) (Figure 7K). In separate cohorts of mice (without implanted electrodes), we confirmed that this deficit following Mrf deletion is specific to remote memory and not caused by expression of the cre^{ERTM} transgene in OPCs (Figures S7H–S7K). Together, these results indicate that oligodendrogenesis is necessary for learning-induced increases in coordinated activity between the hippocampus and prefrontal cortex and suggest that this is a primary mechanism by which disrupting post-training oligodendrogenesis disrupts contextual and spatial memory consolidation.

DISCUSSION

Activity-dependent changes in myelin patterning have been hypothesized to promote coordinated reactivation of neural patterns in distributed cortical regions that are important for the gradual consolidation of initially hippocampus-dependent memories (Pajevic et al., 2014). Here we tested this hypothesis and provide four lines of evidence that indicate that oligodendrogenesis critically contributes to long-term memory consolidation in the adult brain. First, in adult WT mice, we found that spatial learning in the water maze induces oligodendrogenesis. The generation of new oligodendrocytes occurred during training and, additionally, in the immediate post-training period in the absence of any additional training. These changes were largely restricted to cortical and associated white matter regions that have been previously associated with long-term consolidation of spatial information. Second, preventing oligodendrogenesis either during training or immediately following training (but not at more remote time points) impaired consolidation of spatial memories. Third, suppression of oligodendrogenesis similarly impaired consolidation of contextual fear memories. Fourth, contextual fear training increased coupling of hippocampal sharp wave ripples and cortical spindles, two rhythmic oscillations that contribute to memory consolidation. Suppressing oligodendrogenesis prevented these learning-induced increases in oscillatory coupling and impaired consolidation of contextual fear memory. Previous studies have focused on how neuronal changes, whether at the molecular, cellular, or population level (Josselyn et al., 2015; Tonegawa et al., 2018), contribute to memory consolidation. The current data support the idea that non-neuronal cell types contribute critically to consolidation by fine-tuning active circuits following learning (Figure 8).

In the adult brain, oligodendrogenesis is regulated by ongoing neuronal activity. OPCs respond to local neuronal activity by proliferating (Barres and Raff, 1993; Geraghty et al., 2019; Gibson et al., 2014) and differentiating into oligodendrocytes, with myelin formation restricted to a 5-h window following differentiation (Czopka et al., 2013; Demerens et al., 1996; Gibson et al., 2014; Xiao et al., 2016). Furthermore, new oligodendrocytes preferentially myelinate active axons (Mitew et al., 2018), and neuronal activity determines the number of sheaths formed, as well as their stability (Hines et al., 2015; Mensch et al., 2015). Based on this, we hypothesized that neuronal activity in circuits engaged in encoding and consolidation of spatial memories would promote oligodendrogenesis. Consistent with this, we found that spatial learning induced oligodendrogenesis during training and during the period immediately following training. Neuronal activity during these periods is likely detected by OPCs' ongoing surveillance of their surroundings, allowing them to proliferate and/or differentiate into oligodendrocytes on demand (Geraghty et al., 2019; Hughes et al., 2013). Moreover, the nearly uniform distribution of OPCs across the brain, particularly in the cortex (Hughes et al., 2013), indicates that there is a large potential for experience-dependent tuning of cortical networks following learning (Hughes et al., 2018). Consistent with this, cortical oligodendrocytes accumulate over adulthood (Hill et al., 2018; Hughes et al., 2018; Yakovlev and Lecours, 1967), and the human cerebral cortex exhibits a 2.5% yearly addition of oligodendrocytes in adulthood (Yeung et al., 2014).

To assess whether these experience-driven changes in oligodendrogenesis lead to changes in myelin patterning, we used electron microscopy and quantified the number of myelinated axons (reflecting *de novo* myelination) and myelin thickness (reflecting either alterations in pre-existing myelin or *de novo* myelination). Water maze training increased the number of myelinated axons without affecting myelin thickness. These changes occurred in the *corpus callosum/cingulum*, the same region in which training-related increases in oligodendrogenesis occurred. Importantly, these changes were absent when oligodendrogenesis was blocked. These observations are consistent with findings that (1) sensory experience primarily induces *de novo* myelination rather than affecting existing myelin patterns (Hughes et al., 2018) and (2) cortical myelin remodeling depends almost exclusively on the production of new oligodendrocytes in adult animals (Hill et al., 2018).

Changes in myelin patterning are hypothesized to tune active circuits by promoting coordinated neural activity across brain regions and, in particular, synchronizing rhythmic oscillations (Pajevic et al., 2014). Communication between the CA1 and ACC is coupled through sharp wave ripples in the CA1 and cortical spindles in the ACC (Peyrache et al., 2009, 2011; Siapas and Wilson, 1998). Furthermore, coupling increases following memory encoding (Maingret et al., 2016; Ognjanovski et al., 2017; Xia et al., 2017). Interventions that promote ripple-spindle coupling enhance memory consolidation (Maingret et al., 2016), whereas interventions that impede ripple-spindle coupling impair memory consolidation (Xia et al., 2017). Similarly, following contextual fear conditioning, we observed an increase in ripple-spindle coupling, and, critically, this learning-related increase was prevented in mice in which we blocked oligodendrogenesis. In these same mice, consolidation of contextual fear memory was disrupted.

There are a number of potential mechanisms by which *de novo* myelination might facilitate learning-induced changes in brain synchrony, and we consider two here. First, the timing of ACC spindles and CA1 ripples is modulated by several common drivers (e.g., the *nucleus reuniens* and mediodorsal thalamic nucleus; Li et al., 2004; Xu and Südhof, 2013). One possibility is that learning induces *de novo* myelination in these projections, promoting the synchronized arrival of inputs in the CA1 and ACC and, consequently, increasing the probability of ripple-spindle coupling. Second, roughly half of the myelinated axons in cortical layers 2–4 are on parvalbumin+ (PV), fast-spiking basket cells (Micheva et al., 2016). Furthermore, myelination is increased on these PV cells by neural activity (Stedehouder et al., 2018). Such activity-driven changes in myelin patterning could either provide metabolic support (and help sustain high levels of activity) or change conduction velocity. In particular, two lines of research suggest that changes in metabolic support on PV cells would affect ripple-spindle coupling. First, chemogenetic suppression of PV cell activity in either the hippocampus or cortex reduces the probability of ripple-spindle coupling (and impairs consolidation of contextual fear memory) (Xia et al., 2017). Second, rhythmic activation of PV+ interneurons promotes contextual fear memory and stabilizes CA1 network activity (Ognjanovski et al., 2017, 2018).

An alternative possibility is that *de novo* myelination prevents excessive axonal remodeling, which may perturb, rather than tune, activated circuits. However, a recent study showed that *de novo* myelination occurs on new collaterals rather than at branch points. This suggests that collateralization can still occur, even in the presence of new myelination (Stedehouder et al., 2018).

We observed that oligodendrogenesis was elevated in multiple cortical and associated white matter regions, including prefrontal cortices. Neural activity within prefrontal regions during learning appears to be important for successful long-term consolidation of memories. For example, pharmacological inhibition of activity (±-amino-3-hydroxy-5-methyl-4-isoxazolepropionic acid [AMPA] receptor blockade) or plasticity (N-methyl-D-aspartate [NMDA] receptor blockade) in the orbitofrontal cortex during social transmission of food preference training disrupts subsequent memory expression at remote time points (Lesburguères et al., 2011). Similarly, optogenetic inactivation of amygdala or entorhinal inputs into layer 5 medial prefrontal cortex cells during contextual fear conditioning impairs subsequent memory expression at remote time points (Kitamura et al., 2017). These studies suggest that prefrontal cortical circuits are tagged at the time of training but are not necessarily important for the memory expression at short delays (i.e., recent memory). However, maturation of this tagged “silent” engram in the prefrontal cortex is necessary for memory expression at later time points (i.e., remote memory) (Tonegawa et al., 2018). Oligodendrocytes begin to mature within hours of training (Xiao et al., 2016). Therefore, our data suggest that changes in myelin patterning in cortical and associated white matter regions that are initiated by training are similarly necessary for successful consolidation of spatial memory, perhaps for the formation of this “silent” engram in the prefrontal cortex.

In summary, our paper built on two previous lines of work. First, neural activity promotes oligodendrogenesis and *de novo* myelination in activated circuits (Gibson et al., 2014; Mitew et al., 2018). Second, motor skill learning rapidly induces oligodendrogenesis in the

motor cortex, and blocking oligodendrogenesis impairs motor skill learning (McKenzie et al., 2014; Xiao et al., 2016). In the current study, we show that training similarly induces oligodendrogenesis in circuits related to spatial memory. However, it has been unclear how these changes in behavior are related to oligodendrogenesis and *de novo* myelination. One prominent hypothesis has been that experience-dependent changes in myelination patterns optimize neural communication by synchronizing activity across the brain and that this is crucial for successful learning and memory consolidation. Consistent with this hypothesis, our *in vivo* electrophysiological experiments found that neural communication is optimized by learning, and that these changes depend on oligodendrogenesis. More broadly, our findings support the idea that experience remodels activated circuits via oligodendrogenesis in human and non-human species (Fields, 2008, 2015; Gibson et al., 2018; Mount and Monje, 2017; Sampaio-Baptista and Johansen-Berg, 2017; Zatorre et al., 2012). For example, water maze training alters diffusion tensor imaging signals in the cerebral cortex as well as the *corpus callosum* in mice (Blu-menfeld-Katzir et al., 2011). Similarly, learning to juggle correlates with changes to white matter regions for vision processing in humans (Scholz et al., 2009). Together with the current study, these data support the idea that activity-regulated oligodendrogenesis represents a powerful and under-appreciated mechanism for experience-dependent circuit remodeling in the adult brain, at the time of learning and during post-training periods.

STAR★METHODS

LEAD CONTACT AND MATERIALS AVAILABILITY

Further information and requests for resources and reagents should be directed to and will be fulfilled by the Lead Contact, Paul Frankland (paul.frankland@sickkids.ca). This study did not generate new unique reagents.

EXPERIMENTAL MODEL AND SUBJECT DETAILS

All procedures were conducted in accordance with policies of the Hospital for Sick Children Animal Care Committee and conformed to both Canadian Council on Animal Care (CCAC) and National Institutes of Health (NIH) Guidelines on Care and Use of Laboratory.

Experimental Animals—All experiments were conducted on 10-12-week-old adult mice. Atotal of 6 lines of mice were used. To evaluate oligodendrocyte-lineage cellular proliferation during memory consolidation, we used wild-type (WT) C57BL/6N mice (Taconic Farms, Germantown, NY) derived from a colony maintained at the Hospital for Sick Children.

To test whether deletion of Mrf in OPCs impaired oligodendrogenesis, we used two lines of mice expressing a fluorescent reporter in OPCs. In one line of mice Mrf was present in OPCs while in the second line Mrf was conditionally deleted.

To produce the first line (expressing a fluorescent reporter in OPCs), we crossed transgenic mice in which tamoxifen TAM-dependent recombinase cre^{ERTM} is expressed in NG2-expressing cells (NG2-cre^{ERTM}, strain: 008538) with mice expressing a floxed-stop TdTomato cassette at the Rosa locus (Ai14 or Ai14 B6.Cg-

Gt(ROSA)26Sor$^{tm14(CAG-tdTomato)Hze}$/J, strain 007914). The offspring of these mice were heterozygous for floxed-stop TdTomato and either hemizygous for the NG2-Cre^{ERTM} transgene or wild-type. The hemizygous mice were used (NG2-TdT).

To produce the second line, in which Mrf is deleted from, and a fluorescent reporter is expressed in, OPCs, we used the NG2-cre^{ERTM} and Ai14 lines, as well as a line with a knockin of two loxP sites within the Mrf gene (floxed-Mrf or B6;129-*Myrf*^{tm1Barr}/J, strain: 010607) (Emery et al., 2009). The NG2-cre^{ERTM} line was crossed with the homozygous floxed-Mrf line to generate hemizygous NG2 and heterozygous floxed-Mrf, which were backcrossed to achieve hemizygous NG2 and homozygous floxed-Mrf mice (NG2-Mrf). Separately, homozygous floxed-Mrf mice were crossed with homozygous Ai14 mice, the offspring of which were backcrossed creating homozygous floxed-Mrf and homozygous Ai14 double transgenic mice (Mrf-TdTomato). These Mrf-TdTomato mice were crossed with the NG2-Mrf line. Offspring then were either hemizygous or WT for the NG2 locus, homozygous for floxed-Mrf and heterozygous for TdTomato (NG2-TdT-Mrf). Only mice that were hemizygous for the NG2 locus were used for experiments, except in the *in vivo* electrophysiological experiments where littermates (WT for the NG2 transgene) were used as controls.

To test whether Mrf deletion in OPCs affected memory consolidation, we used two lines of mice. First, we used the NG2-Mrf mice. Mice were homozygous for Mrf, and hemizygous for the NG2-cre^{ERTM}, with littermates (WT at NG2 locus) used as controls.

Second, we used the same strategy but took advantage of a different cre-driver line to create a triple-transgenic line. We crossed transgenic mice in which cre^{ERTM} is expressed in PDGFRα-expressing cells (PDGFRα-cre^{ERTM}, strain: 018280) with homozygous floxed-Mrf mice, and these were backcrossed to created hemizygous PDGFRα-homozygous Mrf mice. Separately, homozygous Mrf mice were crossed with YFP-reporter mice (B6.129X1-Gt(ROSA)26Sor$^{tm1(EYFP)Cos}$/J, strain: 006148) and backcrossed to create homozygous-Mrf and YFP mice. The offspring from these two lines were crossed to create experimental mice that were homozygous for Mrf, heterozygous for the YFP reporter and either WT or hemizygous for PDGFRα-cre^{ERTM} (PDGFRα-YFP-Mrf).

In all experiments, the strain used is listed in the figure and/or text, with the notation Mrf_{CON} representing functional Mrf, and Mrf_{CKO} representing conditional deletion of Mrf.

All mice were bred at The Hospital for Sick Children. The day of birth was designated postnatal day 0 (P0). After weaning at P21, same sex mice were group-housed in standard mouse housing cages (2–5 per cage). Rooms were maintained on a 12 h light/dark cycle and behavioral testing occurred during the light phase of the cycle. Both male and female mice were used in all experiments. Mouse genotypes were determined by PCR analysis of tail DNA samples.

METHOD DETAILS

Administration of TAM—TAM (Toronto Research Chemicals) was prepared from powder the day of experiments in 30 mg aliquots. Anhydrous alcohol (100 ml, Sigma) and

Sunflower Seed Oil (900 mL Sigma) was added and the solution vortexed (1 min) and then ultrasonicated (45 min) until fully dissolved. Injection dose was 180 mg/kg (6 ml/g mouse).

4OHT (Toronto Research Chemicals) was prepared before experiments and stored in aliquots at −20°C for up to 4 weeks. This stock solution was prepared by mixing 4OHT with 100% Anhydrous Ethanol (20 mg/ 500 ml) and vortexed (30 s), then placed in a 50°C chamber for 1.5 h with periodic vortexing. Once dissolved into solution an equal part Cremaphore (20 mg/ 500 ml, Sigma) was added and the solution was vortexed (1 min) then stored at −20°C. On experiment days, the stock solution was thawed and mixed 1:1 with 1× PBS before injection. Injection dose was 50 mg/kg (5 ml/g mouse). Both 4OHT and TAM were stored in light-tight containers.

For water maze experiments using either 4OHT or TAM, the drug was injected 30-60 s after the completion of the last training or probe trial. Injections were intraperitoneal (i.p.). Alternating sides of the abdomen were used for daily injections. For *in vivo* electrophysiology experiments, injections were given 5 min after completion of a recording session. For experiments without a behavioral component, injections were completed at the same hour each day.

Administration of 5-ethynyl-20-deoxyuridine—To examine proliferation and oligodendrogenesis we administered 5-ethynyl-2′-deoxyuridine (EdU, Carbosynth) in drinking water (McKenzie et al., 2014) for 96 h. The EdU was dissolved in water with 0.2 mg/ml of sucrose. Intake was monitored daily to assess whether consistent volumes were consumed across experiments.

Water maze—A circular plastic pool (120 cm diameter) was filled to a depth of 40 cm with water made opaque by nontoxic paint. A circular escape platform (10 cm diameter) was submerged 1 cm below the surface of the water in the center of one of the pool quadrants. The pool was surrounded by visual cues located 1 m from the pool wall which were distinct in color and geometric shape.

For the manipulation of oligodendrogenesis during training, mice were given 3 trials per day for 4 days, with EdU, or 4OHT treatment beginning after the last trial on the first day of training. A probe test was performed 24 h following training completion. For the manipulation of oligodendrogenesis post-training, mice were given 3 trials per day for 6 days, with EdU, TAM, or 4OHT treatment beginning after the last trial on the last day of training. Probe tests were performed 1 d and 28 d following training completion.

Trials started when the mouse was placed in the pool, facing the pool wall from one of 4 starting points. Starting points were randomized across trials. Trials ended when the mouse reached the platform, or 60 s transpired. If a mouse failed to find the platform, it was gently guided by the experimenter and kept on the platform for 15 s. If the mouse found the platform during a trial it was allowed to stay on the platform for 15 s before being removed from the pool. During a probe test, the platform was removed and the mouse searched the pool for 60 s. Mouse position was recorded with an overhead camera and tracked using WaterMaze software (Actimetrics). Time spent in a circular zone (20 cm radius) centered on

the platform location was measured during probe tests. Density plots showing search areas were generated using custom python code developed from positional data.

Contextual fear conditioning and testing—Contextual fear conditioning and testing was performed in stainless steel chambers (31 × 24 × 21 cm; Med Associates, St. Albans, VT). The floor comprised of metal bars (3.2 mm diameter) at 7.9 mm intervals. The front and back of the chamber were made of clear acrylic whereas the two sides were made of metal. An overhead camera monitored behavior and freezing was scored automatically with Freezeframe software (Actimetrics).

Animals were conditioned using 3 unsignaled foot-shocks of 0.5 mA for 2 s. The shocks were preceded by a 2-minute period and a 1-minute period after each shock, resulting in a 5-minute conditioning session. Mice were then returned to their home cage. Memory was tested 1 or 28 days after training by placing mice back in the chamber for 5 minutes and freezing during this period was assessed.

Perfusion and immunohistochemistry—Following completion of the experiment, mice were deeply anesthetized with chloral hydrate and perfused transcardially with 20 mL of ice cold 1× PBS followed by 20 mL of 4% PFA at a rate of 0.1 mL per s. For electron microscopy experiments, instead of 4% PFA, a 2% PFA and 2.5% glutaraldehyde solution in 0.1 M sodium cacodylate buffer was used.

For water maze experiments, mice were perfused 1 h following the final probe test. After perfusion, the brain was removed and placed in 4% PFA (20 ml) and post-fixed at 4°C shaking for 24 h. Intact brains were then washed in 1× PBS and stored up to 1 month at 4°C. Before sectioning, brains were placed in 30% sucrose 1× PBS solution for 3 days shaking for cryoprotection. Brains were then coronally sectioned at a thickness of 50 mm using a cryostat (Leica CM1850), collecting sections at approximately 1.8 mm, 1.1 mm, −1.5 mm, −2 mm, −2.5 mm and −4.4 mm from Bregma.

To analyze proliferation and oligodendrogenesis with EdU, the click reaction was carried out by preparing the click solution and 1 M Ascorbic acid to catalyze. The click solution consisted of 10 mM $CuSO_4$-$5H_2O$ (Sigma, 200 ml/ml), 1 M Tris-pH 8.5 (Sigma, 100 ml/ml), H_2O (599 ml/ml), and 10 mM sulfo-cyanine3-azide (Lumiprobe, 1 ml/ml). This click solution was added first to free floating slices and incubated for 5 minutes. Then 1 M Ascorbic acid was prepared fresh from powder and 100 mL per ml of total solution (click solution + ascorbic acid) was added to each well. The total solution was left at room temperature shaking for 1.5 h. Sections were then washed with 1× PBS (3 times).

To analyze OPCs, sections were blocked in 1× PBS with 10% Normal Donkey Serum (NDS) and 0.3% Triton X-100 overnight shaking at room temperature. After, sections were incubated in PBS containing 10% NDS, 0.3% Triton X-100, rabbit polyclonal anti-Olig2 primary antibody (1:500 dilution, Millipore AB9610) and goat polyclonal anti-PDGFRα primary antibody (1:500 dilution, R&Dsystems AF1062)for24 h at room temperature. Sections were washed with 1× PBS (3 times) and then incubated in PBS with secondary antibodies donkey anti-goat Alexa Fluor 488 or 674 (1:500 dilution, Thermo Fisher

Scientific A-11055 or A-21447) and donkey anti-rabbit Alexa Fluor 488 or 647 (1:500, Thermo Fisher Scientific A-31573 or A-21206) for 2 h at room temperature.

To analyze oligodendrocytes, sections were incubated in 40% methanol solution for 1.5 h before blocking (same blocking solution as above). Sections were then incubated with primary antibody mouse monoclonal anti-CC1 (1:200 dilution, Calbiochem OP80) and rabbit polyclonal anti-Olig2 primary antibody (1:500 dilution, Millipore AB9610) for 24 h at room temperature. Sections were washed with 1× PBS (3 times) and then incubated in PBS with secondary antibodies donkey anti-mouse Alexa Fluor 488 (1:500 dilution Thermo Fisher Scientific A-21202) and donkey anti-rabbit Alexa Fluor 488 or 647 (1:500, Thermo Fisher Scientific A-31573) for 2 h at room temperature.

To analyze neurons and astrocytes, sections were blocked in 1× PBS with 10% Normal Donkey Serum (NDS) and 0.3% Triton X-100 overnight shaking at room temperature. After, sections were incubated in PBS containing 10% NDS, 0.3% Triton X-100, rabbit polyclonal anti-GFAP primary antibody (1:1000 dilution, Millipore DAKO Z0334) and mouse monoclonal anti-NeuN primary antibody (1:1000 dilution, Millipore AB377) for 24 h at room temperature. Sections were washed with 1× PBS (3 times) and then incubated in PBS with secondary antibodies donkey anti-mouse Alexa Fluor 488 (1:500 dilution, Thermo Fisher Scientific A-11055) and donkey anti-rabbit Alexa Fluor 647 (1:500, Thermo Fisher Scientific A-21206) for 2 h at room temperature.

All stained sections were washed with 1× PBS (3 times) with one wash including DAPI (1:10,000, Sigma), then mounted on gel-coated slides and coverslipped using PermaFluor mounting medium.

Confocal microscopy—Sections were imaged using a laser-scanning confocal microscope (Zeiss LSM 710). For figure presentation of IHC, 40X magnification images were acquired from the region of interest. For cell quantification, images were acquired at 20X magnification covering the region of interest. Imaging and analysis were performed blind to experimental conditions. For experiments, TdTomato or EdU cells were counted first then those labeled with Olig2 were counted. For $TdTomato^+/Olig2^+$ or $EdU^+/Olig2^+$ cells, we then evaluated CC1 (oligodendrocytes) or PDGFRα (oligodendrocyte-precursor cells, OPCs) expression. To assess recombination rates in OPCs, all $TdTomato^+/Olig2^+/PDGFR\alpha^+$ cells were counted, and this was divided by the number of $Olig2^+/PDGFR\alpha^+$ cells. To assess existing oligodendrocytes, all $Olig2^+$ cells were counted and the density of $Olig2^+/TdTomato^+$cells was subtracted from the total $Olig2^+$ cell density to determine the density of $Olig2^+$ cells not labeled by TdTomato. To assess whether recombined cells included neurons or astrocytes, TdTomato cells were counted first then either NeuN or GFAP for neurons and astrocytes respectively. All cell counts were normalized to the area quantified to yield cell densities, with 1-2 sections/mouse quantified for 3-9 mice/group. Analysis was performed using FIJI software (National Institute of Health).

Electron microscopy—Regions of interest were trimmed using a brain matrix and razor blades and left in 2% PFA and 2.5% glutaraldehyde solution in 0.1 M sodium cacodylate buffer for up to 1 week at 4°C. Samples were rinsed and post-fixed in 1% osmium tetroxide,

then dehydrated in ethanol and embedded in Quetol-Spurr resin at 65°C overnight. Using an ultramicrotome (Leica EM UC7), 90 nm sections were cut and stained with uranyl acetate and lead citrate. Images were then acquired using a Tecnai 20 TEM. Quantification was performed using FIJI software (National Institute of Health). Imaging and analysis were performed blind to experimental conditions. For g-ratio, the axon diameter was measured at the narrowest point and then the diameter including the myelin sheaths. The g-ratio was computed as the axon diameter divided by the axon with myelin sheath diameter.

***In vivo* electrophysiology—**At 10-12 weeks of age, NG2-Mrf-TdTomato mice were implanted with custom-made local field potential (LFP) electrodes in the ACC (+0.8 mm AP, ± 0.3 mm ML, −1.8 mm DV) and CA1 (−1.9 mm AP, ±1.3 mm ML, −1.7 mm DV). Mice were first administered atropine sulfate (0.1 mg/kg, i.p.), then anesthetized with chloral hydrate (400 mg/kg, i.p.). Mice were then placed in a stereotaxic frame. Three small stainless-steel screws were placed in the skull, including one in the skull above the cerebellum for ground. A stripped stainless-steel wire was inserted into the neck muscle for recording electromyogram (EMG) activity. Holes were drilled in the skull at the target coordinates and custom made Teflon-coated stainless steel LFP electrodes (A-M Systems, Carlsborg, WA) bundled in 23–25G stainless steel cannulas were slowly lowered to the ACC (bipolar electrode with 0.5 mm distance between electrodes) and CA1 (tripolar electrode with 0.3 mm distance between electrodes), at the rate of 0.1 mm/s. This allowed LFP signals to be referenced locally within the target region during surgery. All wires were soldered to gold pins on a custom-made board and connector (Omnetics) which was secured using dental cement. Mice were given ketoprofen (5 mg/kg, s.c.) and 1 mL 0.9% saline (s.c.). Mice were single-housed after surgery to minimize damage to the electrode cap.

Three days after surgery, mice were habituated to the recording chamber for 2 h. The recording chamber was a dimly lit, sound-attenuated chamber, in which the mouse and a 20.3 (h) × 15.25 (I) × 15.25 (w) cm opaque plastic chamber were placed. Recording sessions were carried out using the Neuralynx Cheetah system. Signal was amplified 1000 times, filtered between 1 and 1000 Hz, and digitized at 2 kHz. On the following day, baseline LFP activity was collected for 3 h. Following this, the first 4OHT injection was given (followed by 3 more daily 4OHT injections). Five days later mice underwent contextual fear conditioning (see contextual fear conditioning section for protocol) and 5 minutes later placed in chamber and LFP signals were recorded for 3-4 h. Contextual fear memory was then assessed 28 days after training.

At the end of the experiments, electrolytic lesions (20 μA for 30 s) were created to verify the locations of electrodes. One-week later, mice were transcardially perfused, and the brains were sectioned and imaged to verify electrode placement. We used DAPI staining to identify the lesion and region.

QUANTIFICATION AND STATISTICAL ANALYSIS

Electrophysiological analysis—Analysis was performed offline using MATLAB (The MathWorks) with established methods as described below.

The detection criteria for ripples and spindles were similar to previously used settings (Eschenko et al., 2006; Xia et al., 2017) and were verified manually for the current dataset. Ripples were detected by band-pass filtering (150-250 Hz) the CA1 pyramidal cell layer electrode signal and amplitude were calculated using the Hilbert transform. Ripple windows were defined as signals with an amplitude four times the standard deviation. Spindles were detected from the ACC electrodes using a band-pass filter (12-15 Hz), and again calculated amplitude with the Hilbert transform. Spindle windows were signals two times the standard deviation with a duration of 200-2000 ms. Ripple and spindle density where calculated by dividing the number of events by the NREM duration, calculated for each mouse and session. The ripple and spindle amplitude were computed by taking the peak instantaneous amplitude during each ripple or spindle window and averaging it across the number of events for each recording session. The ripple and spindle amplitudes and densities were normalized within mouse to the respective values from the baseline recording session.

The amount of recording time in NREM sleep stage was determined using adaptive theta/delta ratio (Klausberger et al., 2003)(threshold = 3.5 × mode) extracted from power spectrums during the periods where the mouse is immobile (EMG amplitude < 5 × mode). Low theta/delta ratio (below threshold) is indicative of NREM periods.

To specifically assess the coupling of ripples in CA1 with spindles in ACC, we calculated the ripple-spindle joint occurrence. This was defined as ripple events that occur within ± 90 ms time window from spindle center (Maingret et al., 2016; Xia et al., 2017). This was normalized to the total number of spindle events within the recording session. The values for post-training sessions were normalized to the joint occurrence rate during the pre-training baseline recording session.

To more precisely assess temporal coupling of ripples and spindles, we cross-correlated the instantaneous amplitudes of ripple and spindle amplitudes (Adhikari et al., 2010; Xia et al., 2017). Specifically, during NREM sleep periods, we performed cross-correlation of the ripple and spindle amplitude in a ± 2 s time window from spindle center with 0.01 s sliding time window increments. Lag between ripple-spindle peak correlation and spindle center was calculated, where a positive lag indicates a spindle lead.

Statistical analysis—No statistical tests were used to pre-determine sample size, however sample sizes are consistent with similar published experiments. Data are presented as the mean ± s.e.m. across all experiments. Data were analyzed using parametric two-way repeated-measures ANOVA, two-way ANOVA, or two-sample Student's unpaired t test. For comparisons between two groups, if the groups had significantly different variances (with $\alpha = 0.05$), Welch's t test was used. For post hoc tests, Tukey HSD was used and corrected using the False Discovery Rate method.

DATA AND CODE AVAILABILITY

Requests should be directed to the lead contact. The datasets generated during this study are available at Mendeley datasets: https://data.mendeley.com/datasets/sy26r6ny66/1

Supplementary Material

Refer to Web version on PubMed Central for supplementary material.

ACKNOWLEDGMENTS

This work was supported by Canadian Institutes of Health Research (CIHR) grants FDN143227 and PJT156164 (to P.W.F. and MOP74650 (to S.A.J.). S.A.J. is a CIHR Canada Research Chair in Memory Function and Dysfunction. P.W.F. is a CIHR Canada Research Chair in Cognitive Neurobiology. P.E.S. was supported by a CIHR Vanier graduate scholarship, an Arnie Aberman fellowship, and a McLaughlin MD/PhD studentship. We thank Doug Holmyard and Ali Darbandi at the Nanoscale Biomedical Imaging Facility at The Hospital for Sick Children for assistance with electron microscopy. We also thank Lina Tran for development of the Python code for density plots of the water maze data.

REFERENCES

Adhikari A, Sigurdsson T, Topiwala MA, and Gordon JA (2010). Cross-correlation of instantaneous amplitudes of field potential oscillations: a straightforward method to estimate the directionality and lag between brain areas. J. Neurosci. Methods 191, 191–200. [PubMed: 20600317]

Barres BA, and Raff MC (1993). Proliferation of oligodendrocyte precursor cells depends on electrical activity in axons. Nature 361, 258–260. [PubMed: 8093806]

Blumenfeld-Katzir T, Pasternak O, Dagan M, and Assaf Y (2011). Diffusion MRI of structural brain plasticity induced by a learning and memory task. PLoS ONE 6, e20678. [PubMed: 21701690]

Boyce R, Glasgow SD, Williams S, and Adamantidis A (2016). Causal evidence for the role of REM sleep theta rhythm in contextual memory consolidation. Science 352, 812–816. [PubMed: 27174984]

Buzsáki G (1996). The hippocampo-neocortical dialogue. Cereb. Cortex 6, 81–92. [PubMed: 8670641]

Carr MF, Jadhav SP, and Frank LM (2011). Hippocampal replay in the awake state: a potential substrate for memory consolidation and retrieval. Nat. Neurosci 14, 147–153. [PubMed: 21270783]

Czopka T, Ffrench-Constant C, and Lyons DA (2013). Individual oligodendrocytes have only a few hours in which to generate new myelin sheaths in vivo. Dev. Cell 25, 599–609. [PubMed: 23806617]

Demerens C, Stankoff B, Logak M, Anglade P, Allinquant B, Couraud F, Zalc B, and Lubetzki C (1996). Induction of myelination in the central nervous system by electrical activity. Proc. Natl. Acad. Sci. USA 93, 9887–9892. [PubMed: 8790426]

Diekelmann S, and Born J (2010). The memory function of sleep. Nat. Rev. Neurosci 11, 114–126. [PubMed: 20046194]

Emery B, Agalliu D, Cahoy JD, Watkins TA, Dugas JC, Mulinyawe SB, Ibrahim A, Ligon KL, Rowitch DH, and Barres BA (2009). Myelin gene regulatory factor is a critical transcriptional regulator required for CNS myelination. Cell 138, 172–185. [PubMed: 19596243]

Eschenko O, Mölle M, Born J, and Sara SJ (2006). Elevated sleep spindle density after learning or after retrieval in rats. J. Neurosci 26, 12914–12920. [PubMed: 17167082]

Fields RD (2008). White matter in learning, cognition and psychiatric disorders. Trends Neurosci. 31, 361–370. [PubMed: 18538868]

Fields RD (2015). A new mechanism of nervous system plasticity: activity-dependent myelination. Nat. Rev. Neurosci 16, 756–767. [PubMed: 26585800]

Geraghty AC, Gibson EM, Ghanem RA, Greene JJ, Ocampo A, Goldstein AK, Ni L, Yang T, Marton RM, Paşca SP, et al. (2019). Loss of Adaptive Myelination Contributes to Methotrexate Chemotherapy-Related Cognitive Impairment. Neuron 103, 250–265.e8. [PubMed: 31122677]

Gibson EM, Purger D, Mount CW, Goldstein AK, Lin GL, Wood LS, Inema I, Miller SE, Bieri G, Zuchero JB, et al. (2014). Neuronal activity promotes oligodendrogenesis and adaptive myelination in the mammalian brain. Science 344, 1252304. [PubMed: 24727982]

Gibson EM, Geraghty AC, and Monje M (2018). Bad wrap: Myelin and myelin plasticity in health and disease. Dev. Neurobiol 78, 123–135. [PubMed: 28986960]

Hill RA, Li AM, and Grutzendler J (2018). Lifelong cortical myelin plasticity and age-related degeneration in the live mammalian brain. Nat. Neurosci 21, 683–695. [PubMed: 29556031]

Hines JH, Ravanelli AM, Schwindt R, Scott EK, and Appel B (2015). Neuronal activity biases axon selection for myelination in vivo. Nat. Neurosci 18, 683–689. [PubMed: 25849987]

Hughes EG, Kang SH, Fukaya M, and Bergles DE (2013). Oligodendrocyte progenitors balance growth with self-repulsion to achieve homeostasis in the adult brain. Nat. Neurosci 16, 668–676. [PubMed: 23624515]

Hughes EG, Orthmann-Murphy JL, Langseth AJ, and Bergles DE (2018). Myelin remodeling through experience-dependent oligodendrogenesis in the adult somatosensory cortex. Nat. Neurosci 21, 696–706. [PubMed: 29556025]

Josselyn SA, Köhler S, and Frankland PW (2015). Finding the engram. Nat. Rev. Neurosci 16, 521–534. [PubMed: 26289572]

Kang SH, Fukaya M, Yang JK, Rothstein JD, and Bergles DE (2010). NG2+ CNS glial progenitors remain committed to the oligodendrocyte lineage in postnatal life and following neurodegeneration. Neuron 68, 668–681. [PubMed: 21092857]

Kitamura T, Ogawa SK, Roy DS, Okuyama T, Morrissey MD, Smith LM, Redondo RL, and Tonegawa S (2017). Engrams and circuits crucial for systems consolidation of a memory. Science 356, 73–78. [PubMed: 28386011]

Klausberger T, Magill PJ, Márton LF, Roberts JDB, Cobden PM, Buzsáki G, and Somogyi P (2003). Brain-state- and cell-type-specific firing of hippocampal interneurons in vivo. Nature 421, 844–848. [PubMed: 12594513]

Lesburguères E, Gobbo OL, Alaux-Cantin S, Hambucken A, Trifilieff P, and Bontempi B (2011). Early tagging of cortical networks is required for the formation of enduring associative memory. Science 331, 924–928. [PubMed: 21330548]

Li XB, Inoue T, Nakagawa S, and Koyama T (2004). Effect of mediodorsal thalamic nucleus lesion on contextual fear conditioning in rats. Brain Res. 1008, 261–272. [PubMed: 15145764]

Maingret N, Girardeau G, Todorova R, Goutierre M, and Zugaro M (2016). Hippocampo-cortical coupling mediates memory consolidation during sleep. Nat. Neurosci 19, 959–964. [PubMed: 27182818]

McKenzie IA, Ohayon D, Li H, de Faria JP, Emery B, Tohyama K, and Richardson WD (2014). Motor skill learning requires active central myelination. Science 346, 318–322. [PubMed: 25324381]

Mensch S, Baraban M, Almeida R, Czopka T, Ausborn J, El Manira A, and Lyons DA (2015). Synaptic vesicle release regulates myelin sheath number of individual oligodendrocytes in vivo. Nat. Neurosci 18, 628–630. [PubMed: 25849985]

Micheva KD, Wolman D, Mensh BD, Pax E, Buchanan J, Smith SJ, and Bock DD (2016). A large fraction of neocortical myelin ensheathes axons of local inhibitory neurons. eLife 5, 3347.

Mitew S, Gobius I, Fenlon LR, McDougall SJ, Hawkes D, Xing YL, Bujalka H, Gundlach AL, Richards LJ, Kilpatrick TJ, et al. (2018). Pharmacogenetic stimulation of neuronal activity increases myelination in an axon-specific manner. Nat. Commun 9, 306. [PubMed: 29358753]

Mount CW, and Monje M (2017). Wrapped to Adapt: Experience-Dependent Myelination. Neuron 95, 743–756. [PubMed: 28817797]

Ognjanovski N, Schaeffer S, Wu J, Mofakham S, Maruyama D, Zochowski M, and Aton SJ (2017). Parvalbumin-expressing interneurons coordinate hippocampal network dynamics required for memory consolidation. Nat. Commun 8, 15039. [PubMed: 28382952]

Ognjanovski N, Broussard C, Zochowski M, and Aton SJ (2018). Hippocampal Network Oscillations Rescue Memory Consolidation Deficits Caused by Sleep Loss. Cereb. Cortex 28, 3711–3723. [PubMed: 30060138]

Pajevic S, Basser PJ, and Fields RD (2014). Role of myelin plasticity in oscillations and synchrony of neuronal activity. Neuroscience 276, 135–147. [PubMed: 24291730]

Peyrache A, Khamassi M, Benchenane K, Wiener SI, and Battaglia FP (2009). Replay of rule-learning related neural patterns in the prefrontal cortex during sleep. Nat. Neurosci 12, 919–926. [PubMed: 19483687]

Peyrache A, Battaglia FP, and Destexhe A (2011). Inhibition recruitment in prefrontal cortex during sleep spindles and gating of hippocampal inputs. Proc. Natl. Acad. Sci. USA 108, 17207–17212. [PubMed: 21949372]

Rivers LE, Young KM, Rizzi M, Jamen F, Psachoulia K, Wade A, Kessaris N, and Richardson WD (2008). PDGFRA/NG2 glia generate myelinating oligodendrocytes and piriform projection neurons in adult mice. Nat. Neurosci 11, 1392–1401. [PubMed: 18849983]

Sampaio-Baptista C, and Johansen-Berg H (2017). White Matter Plasticity in the Adult Brain. Neuron 96, 1239–1251. [PubMed: 29268094]

Scholz J, Klein MC, Behrens TEJ, and Johansen-Berg H (2009). Training induces changes in white-matter architecture. Nat. Neurosci 12, 1370–1371. [PubMed: 19820707]

Siapas AG, and Wilson MA (1998). Coordinated interactions between hippocampal ripples and cortical spindles during slow-wave sleep. Neuron 21, 1123–1128. [PubMed: 9856467]

Stedehouder J, Brizee D, Shpak G, and Kushner SA (2018). Activity-dependent myelination of parvalbumin interneurons mediated by axonal morphological plasticity. J. Neurosci 38, 3631–3642. [PubMed: 29507147]

Takehara-Nishiuchi K (2014). Entorhinal cortex and consolidated memory. Neurosci. Res 84, 27–33. [PubMed: 24642278]

Takeuchi T, Duszkiewicz AJ, and Morris RGM (2013). The synaptic plasticity and memory hypothesis: encoding, storage and persistence. Philos. Trans. R. Soc. Lond. B Biol. Sci 369, 20130288. [PubMed: 24298167]

Teixeira CM, Pomedli SR, Maei HR, Kee N, and Frankland PW (2006). Involvement of the anterior cingulate cortex in the expression of remote spatial memory. J. Neurosci 26, 7555–7564. [PubMed: 16855083]

Tomassy GS, Berger DR, Chen H-H, Kasthuri N, Hayworth KJ, Vercelli A, Seung HS, Lichtman JW, and Arlotta P (2014). Distinct profiles of myelin distribution along single axons of pyramidal neurons in the neocortex. Science 344, 319–324. [PubMed: 24744380]

Tonegawa S, Morrissey MD, and Kitamura T (2018). The role of engram cells in the systems consolidation of memory. Nat. Rev. Neurosci 19, 485–498. [PubMed: 29970909]

Vetere G, Restivo L, Cole CJ, Ross PJ, Ammassari-Teule M, Josselyn SA, and Frankland PW (2011). Spine growth in the anterior cingulate cortex is necessary for the consolidation of contextual fear memory. Proc. Natl. Acad. Sci. USA 108, 8456–8460. [PubMed: 21531906]

Vetere G, Kenney JW, Tran LM, Xia F, Steadman PE, Parkinson J, Josselyn SA, and Frankland PW (2017). Chemogenetic Interrogation of a Brain-wide Fear Memory Network in Mice. Neuron 94, 363–374.e4. [PubMed: 28426969]

Wake H, Lee PR, and Fields RD (2011). Control of local protein synthesis and initial events in myelination by action potentials. Science 333, 1647–1651. [PubMed: 21817014]

Xia F, Richards BA, Tran MM, Josselyn SA, Takehara-Nishiuchi K, and Frankland PW (2017). Parvalbumin-positive interneurons mediate neocortical-hippocampal interactions that are necessary for memory consolidation. eLife 6, 191.

Xiao L, Ohayon D, McKenzie IA, Sinclair-Wilson A, Wright JL, Fudge AD, Emery B, Li H, and Richardson WD (2016). Rapid production of new oligodendrocytes is required in the earliest stages of motor-skill learning. Nat. Neurosci 19, 1210–1217. [PubMed: 27455109]

Xu W, and Südhof TC (2013). A neural circuit for memory specificity and generalization. Science 339, 1290–1295. [PubMed: 23493706]

Yakovlev PI, and Lecours AR (1967). The myelogenetic cycles of regional maturation of the brain In Regional Development of the Brain in Early Life, Minkowski A, ed. (Boston: Blackwell Scientific), pp. 3–70.

Yeung MSY, Zdunek S, Bergmann O, Bernard S, Salehpour M, Alkass K, Perl S, Tisdale J, Possnert G, Brundin L, et al. (2014). Dynamics of oligodendrocyte generation and myelination in the human brain. Cell 159, 766–774. [PubMed: 25417154]

Zatorre RJ, Fields RD, and Johansen-Berg H (2012). Plasticity in gray and white: neuroimaging changes in brain structure during learning. Nat. Neurosci 15, 528–536. [PubMed: 22426254]

Highlights

- Spatial learning promotes oligodendrogenesis and *de novo* myelination in adult mice
- Spatial learning promotes hippocampal ripple-cortical spindle coupling
- Decreasing adult oligodendrogenesis blocks learning-induced increases in coupling
- Decreasing adult oligodendrogenesis impairs spatial memory consolidation

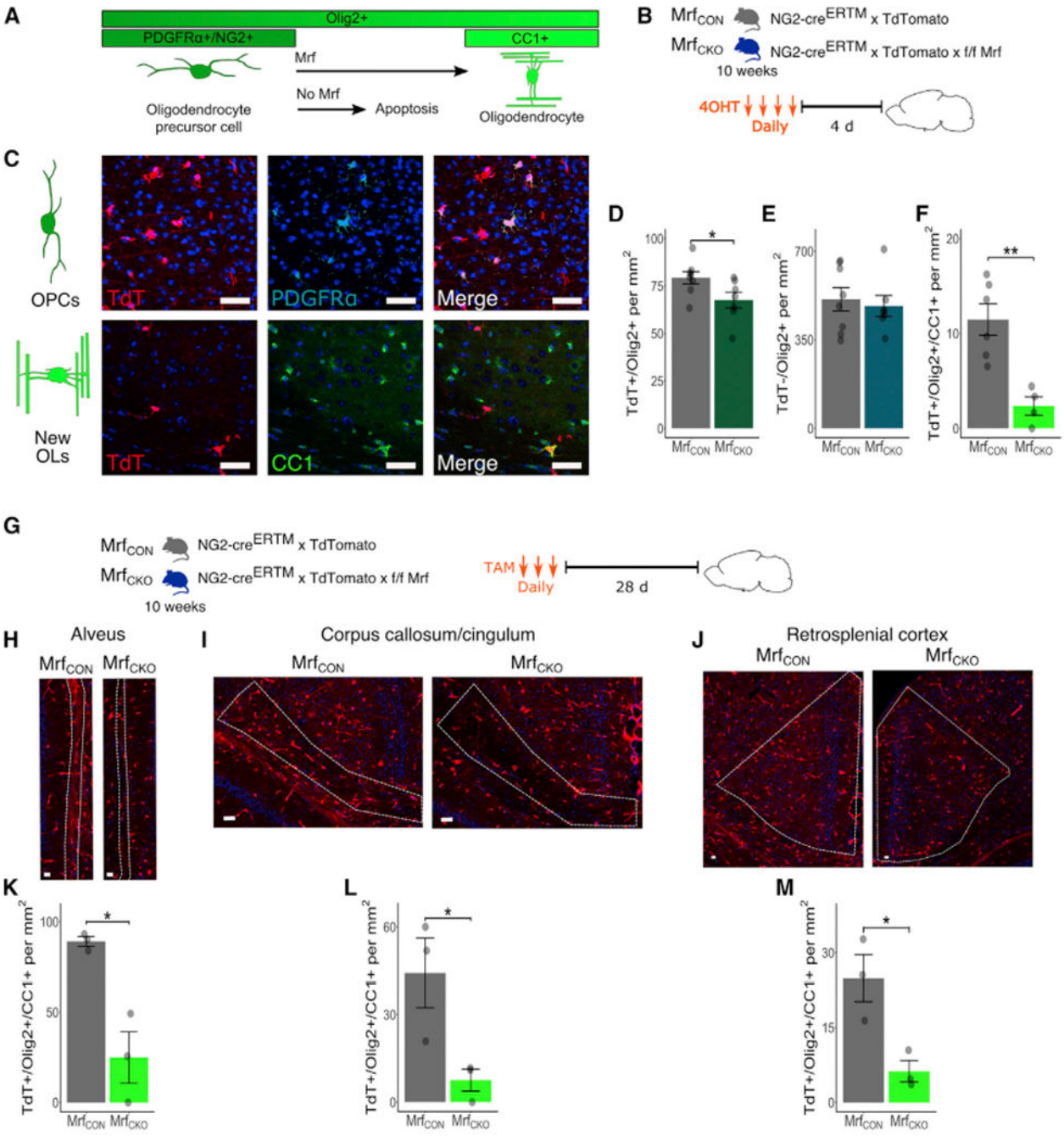

Figure 1. Deletion of Myelin Regulatory Factor (Mrf) in Oligodendrocyte Precursor Cells (OPCs) Disrupts Oligodendrogenesis in the Adult Cortex and *Corpus Callosum* without Affecting Existing Oligodendrocytes

(A) Mrf expression is required for oligodendrocytes to form and maintain myelin.

(B) Top: to examine the role of adult oligodendrogenesis in spatial memory consolidation, we used mice in which TAM or its metabolite 4OHT induces the expression of TdTomato (TdT) and deletes Mrf from OPCs (NG2-cre^{ERTM} × Mrf$^{fl/fl}$ × Ai14 or Mrf$_{CKO}$ mice). NG2-cre^{ERTM} × Ai14 (Mrf$_{CON}$ mice) were controls. Bottom: experimental design. Mrf$_{CON}$ and Mrf$_{CKO}$ mice treated with 4OHT were perfused 4 days later.

(C) Representative images from the retrosplenial cortex, showing co-localization of TdT (a recombination marker) and PDGRFα (an OPC marker) (top) and co-localization of TdT and CC1 (a marker of newly differentiated oligodendrocytes) (bottom).

(D and E) Mrf deletion decreased the density of tagged oligodendrocyte lineage cells (D) but did not affect the density of untagged oligodendrocyte-lineage cells (E) in the retrosplenial cortex, indicating that Mrf deletion in OPCs only affected adult oligodendrogenesis and did not affect existing oligodendrocytes Mrf_{CON} n = 7, Mrf_{CKO} n = 7).

(F) Mrf deletion reduced the number of adult-generated oligodendrocytes (i.e., TdT^+/$Olig2^+$/$CC1^+$ cells).

(G) Experimental design. Adult Mrf_{CON} and Mrf_{CKO} mice treated with TAM were perfused 28 days later.

(H–J) Representative images of TdT^+ cells in the *alveus* (H), *corpus callosum/cingulum* (I), and retrosplenial cortex (J) in Mrf_{CON} and Mrf_{CKO} mice.

(K–M) The density of adult-generated oligodendrocyte (i.e., TdT^+/$Olig2^+$/$CC1^+$) cells was reduced in Mrf_{CKO} mice. in the *alveus* (K), *corpus callosum/cingulum* (L), and retrosplenial cortex (M).

For (H)–(M), Mrf_{CON} n = 3, Mrf_{CKO} n = 3. Scale bars, 20 μm. See also Figure S1. Pooled data are represented as mean ± SEM.

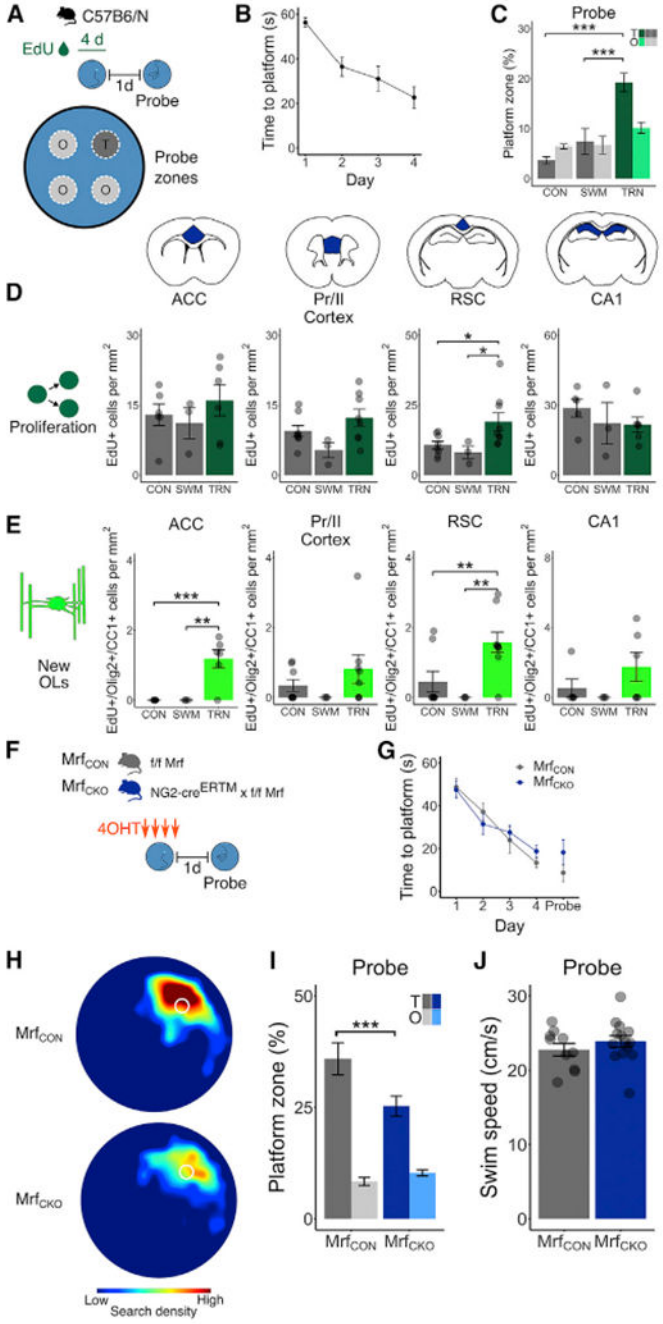

Figure 2. Training-Induced Increases in Oligodendrogenesis Are Necessary for Spatial Learning

(A) Experimental design. Mice were trained in the water maze, and spatial memory was assessed in the probe test 1 day later. Spatial memory was assessed by comparing time in the target (T) zone (centered on platform location during training) versus other (O) equivalent zones in the pool. Mice were treated with EdU during training to assess proliferation of oligodendrocyte lineage cells.

(B) Latency to target platform during training sessions (TRN n = 9).

(C) Percent time spent searching T versus O zones in the probe test (CON n = 16, SWM n = 8, TRN n = 9).
(D) Proliferation (EdU^+ cells) quantified in the anterior cingulate cortex (ACC), prelimbic/infralimbic (Pr/II) cortex, retrosplenial cortex (RSC), and CA1 region of the hippocampus (ACC: CON n = 6, SWM n = 3, TRN n = 6; Pr/II: CON n = 6, SWM n = 3, TRN n = 7; RSC: CON n = 6, SWM n = 3, TRN n = 7; CA1: CON n = 6, SWM n = 3, TRN n = 6).
(E) New oligodendrocytes quantified in the same regions as in (D) (ACC: CON n = 6, SWM n = 3, TRN n = 6; Pr/II: CON n = 6, SWM n = 3, TRN n = 7; RSC: CON n = 6, SWM n = 3, TRN n = 7; CA1: CON n = 6, SWM n = 3, TRN n = 6).
(F) Experimental design. Mrf_{CON} and Mrf_{CKO} were trained in the water maze, and spatial memory was assessed 1 day later. Mice were treated with 4OHT to delete Mrf in OPCs.
(G) During training, Mrf_{CON} (n = 10) and Mrf_{CKO} (n = 14) mice required progressively less time to locate the platform.
(H) Density plot illustrating probe test performance.
(I) Mrf_{CKO} mice searched less selectively compared with Mrf_{CON} mice, spending less time searching the T zone.
(J) Swim speed was equivalent in Mrf_{CON} and Mrf_{CKO} mice during the probe test.
See also Figure S2. Pooled data are represented as mean ± SEM.

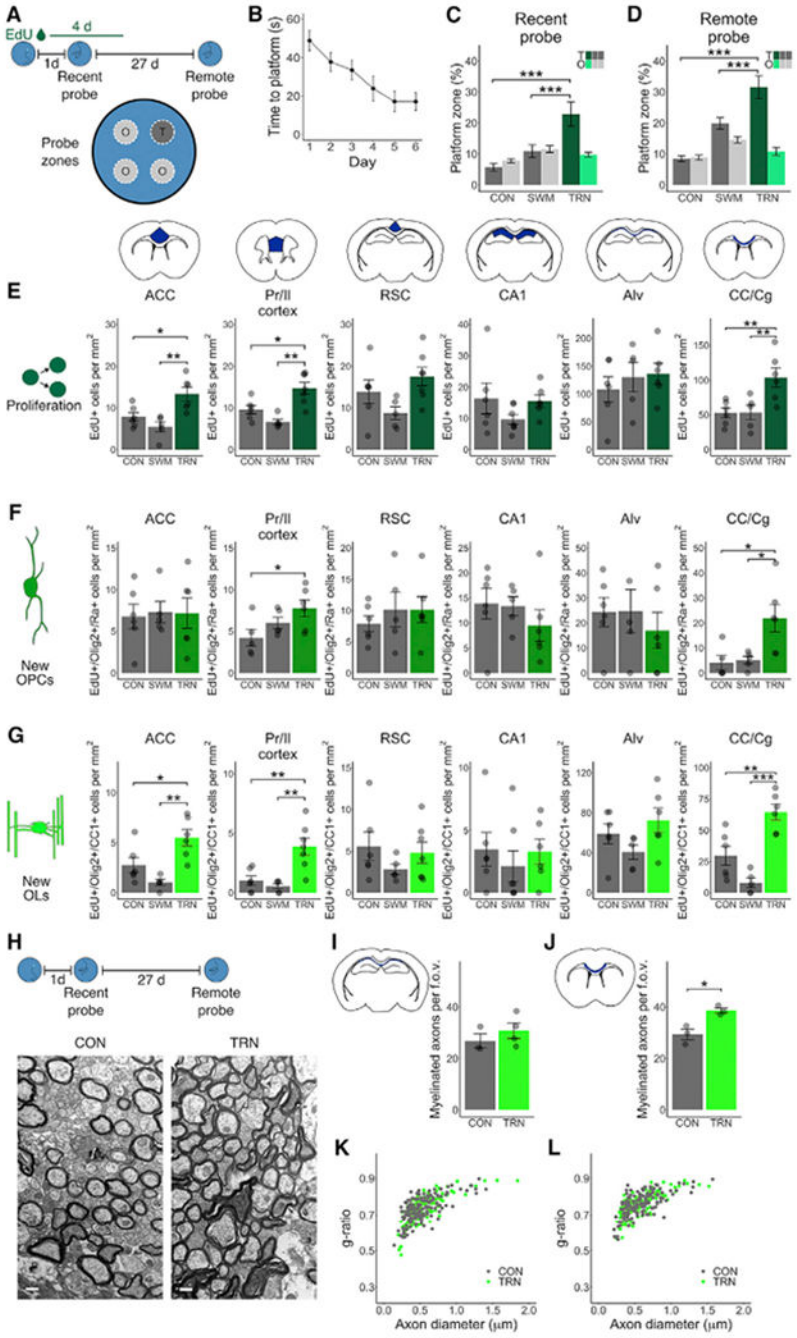

Figure 3. Memory Consolidation Induces Oligodendrogenesis and Myelination in Cortical and White Matter Regions

(A) Experimental design. Mice were trained in the water maze, and spatial memory was assessed in probe tests 1 day and 28 days later. Mice were treated with EdU after training completion to assess proliferation of oligodendrocyte lineage cells.

(B) Latency to target platform during training sessions (TRN n = 8).

(C) Memory probe test search of target zones 1 day after training (CON n = 10, SWM n = 8, TRN n = 8).

(D) Probe test 28 days after training, assessing memory consolidation.

(E) Proliferation (EdU^+ cells) was quantified in the ACC, Pr/Il cortex, RSC, CA1 region of the hippocampus, *alveus* (Alv), and *corpus callosum* (CC)/ *cingulum* (Cg) bordering the cerebral cortex (ACC: CON n = 6, SWM n = 5, TRN n = 6; Pr/II: CON n = 6, SWM n = 5, TRN n = 7; RSC: CON n = 6, SWM n = 5, TRN n = 7; CA1: CON n = 6, SWM n = 6, TRN n = 6; Alv: CON n = 6, SWM n = 5, TRN n = 6; CC/Cg: CON n = 6, SWM n = 5, TRN n = 6).

(F) New OPCs quantified in the same regions as in (E) (ACC: CON n = 6, SWM n = 5, TRN n = 6; Pr/II: CON n = 5, SWM n = 5, TRN n = 6; RSC: CON n = 6, SWM n = 5, TRN n = 6; CA1: CON n = 6, SWM n = 5, TRN n = 6; Alv: CON n = 6, SWM n = 4, TRN n = 6; CC/Cg: CON n = 5, SWM n = 5, TRN n = 6).(G) New oligodendrocytes quantified in same regions as in (E) (ACC: CON n = 6, SWM n = 5, TRN n = 6; Pr/Il: CON n = 6, SWM n = 5, TRN n = 7; RSC: CON n = 6, SWM n = 5, TRN n = 7; CA1: CON n = 6, SWM n = 6, TRN n = 6; Alv: CON n = 6, SWM n = 5, TRN n = 6; CC/Cg: CON n = 6, SWM n = 5, TRN n = 6).

(H) Experimental design. Representative images of myelination content in the *corpus callosum/cingulum* bordering the ACC. Scale bars, 500 nm. (I) Number of myelinated axons per field of view (f.o.v.) in the *alveus* did not change following spatial learning (CON n = 3, TRN n = 4).

(J) The number of myelinated axon f.o.v.s increased in the *corpus callosum/cingulum* after spatial learning (CON n = 3, TRN n = 3).

(K and L) Myelin thickness was unaltered after spatial learning in the *alveus* (K) (CON n = 3, TRN n = 3) and *corpus callosum/cingulum* (L) (CON n = 3, TRN n = 3).

See also Figure S3. Pooled data are represented as mean ± SEM.

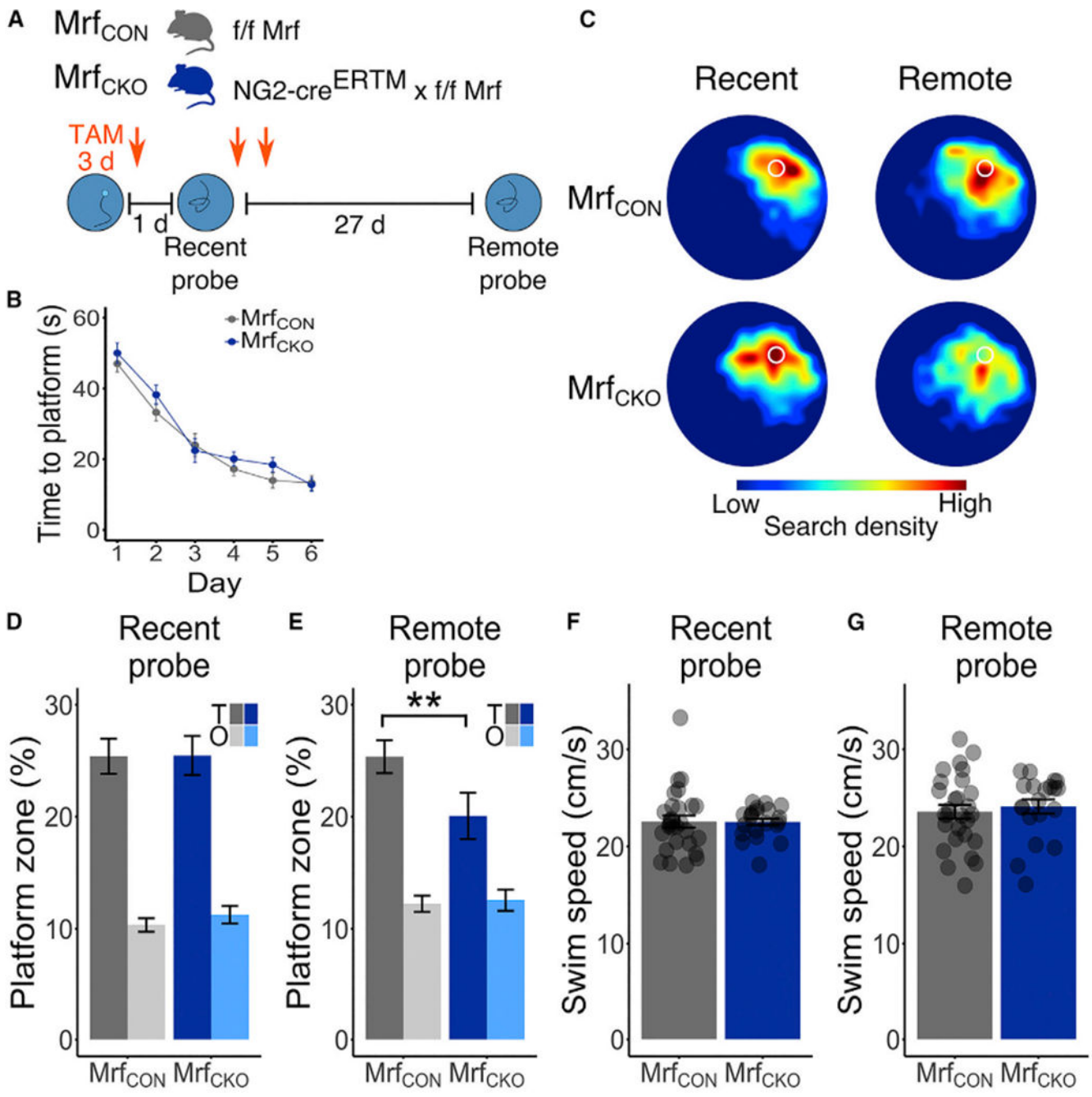

Figure 4. Disruption of Oligodendrogenesis Impairs Memory Consolidation

(A) Experimental design. Mrf$_{CON}$ and Mrf$_{CKO}$ mice were trained in the water maze, and spatial memory was assessed in probe tests 1 day and 28 days later. Mice were treated with TAM, starting immediately after training, to delete Mrf in OPCs.

(B) During training, Mrf$_{CON}$ (n = 28) and Mrf$_{CKO}$ (n = 21) mice required progressively less time to locate the platform.

(C) Density plot illustrating probe test performance in the recent and remote probe test.

(D) In the recent probe test, both Mrf_{CON} and Mrf_{CKO} mice searched selectively, spending more time in the T zone versus O equivalent zones.
(E) In the remote probe test, Mrf_{CKO} mice searched less selectively compared with Mrf_{CON} mice, spending less time searching the T zone.
(F and G) Swim speed was equivalent in Mrf_{CON} and Mrf_{CKO} mice during (F) the recent and (G) remote probe tests.
See also Figure S4. Pooled data are represented as mean ± SEM.

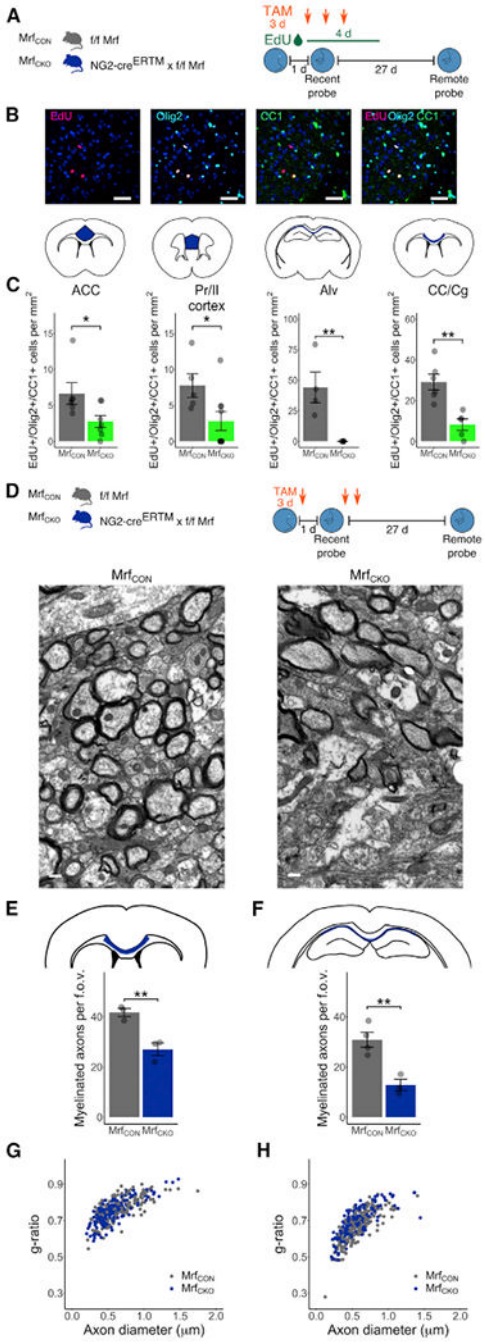

Figure 5. Disruption of Oligodendrogenesis Immediately after Training Blocks Consolidation-Associated Oligodendrogenesis and Myelination

(A) Experimental design. Mrf_{CON} and Mrf_{CKO} mice were trained in the water maze, and spatial memory was assessed in probe tests 1 day and 28 days later. Mice were treated with EdU to assess proliferation of oligodendrocyte lineage cells and TAM to delete Mrf in OPCs, starting immediately after training. See also Figure S5.

(B) EdU^+, $Olig2^+$, and $CC1^+$ cells were assessed in the ACC, Pr/II cortex, Alv, and CC/Cg bordering the cerebral cortex. Representative images are shown for the ACC. Scale bars, 40 μm.

(C) New oligodendrocytes quantified in the ACC, Pr/II, Alv, and CC/Cg (ACC: Mrf_{CON} n = 6, Mrf_{CKO} n = 7; Pr/II: Mrf_{CON} n = 5, Mrf_{CKO} n = 9; Alv: Mrf_{CON} n = 4, Mrf_{CKO} n = 5; CC/Cg: Mrf_{CON} n = 6, Mrf_{CKO} n = 5).

(D) Experimental design. Mrf_{CON} and Mrf_{CKO} mice were trained in the water maze, and spatial memory was assessed in probe tests 1 day and 28 days later. Mice were treated with TAM (to delete Mrf in OPCs), starting immediately after training. A representative electron microscopy (EM) image shows myelinated axons in the *alveus*. Scale bars, 500 nm.

(E and F) Deletion of Mrf in OPCs decreased the number of myelinated axons per f.o.v. in (E) the *corpus callosum/cingulum* (Mrf_{CON} n = 3, Mrf_{CKO} n = 3) and (F) *alveus* (Mrf_{CON} n = 4, Mrf_{CKO} n = 3).

(G and H) Deletion of Mrf in OPCs did not affect the quantified g-ratio of axons in (G) the *corpus callosum/cingulum* (Mrf_{CON} n = 4, Mrf_{CKO} n = 3) and (H) *alveus* (Mrf^{CON}n = 4 Mrf^{CKO} n = 3).

See also Figure S5. Pooled data are represented as mean ± SEM.

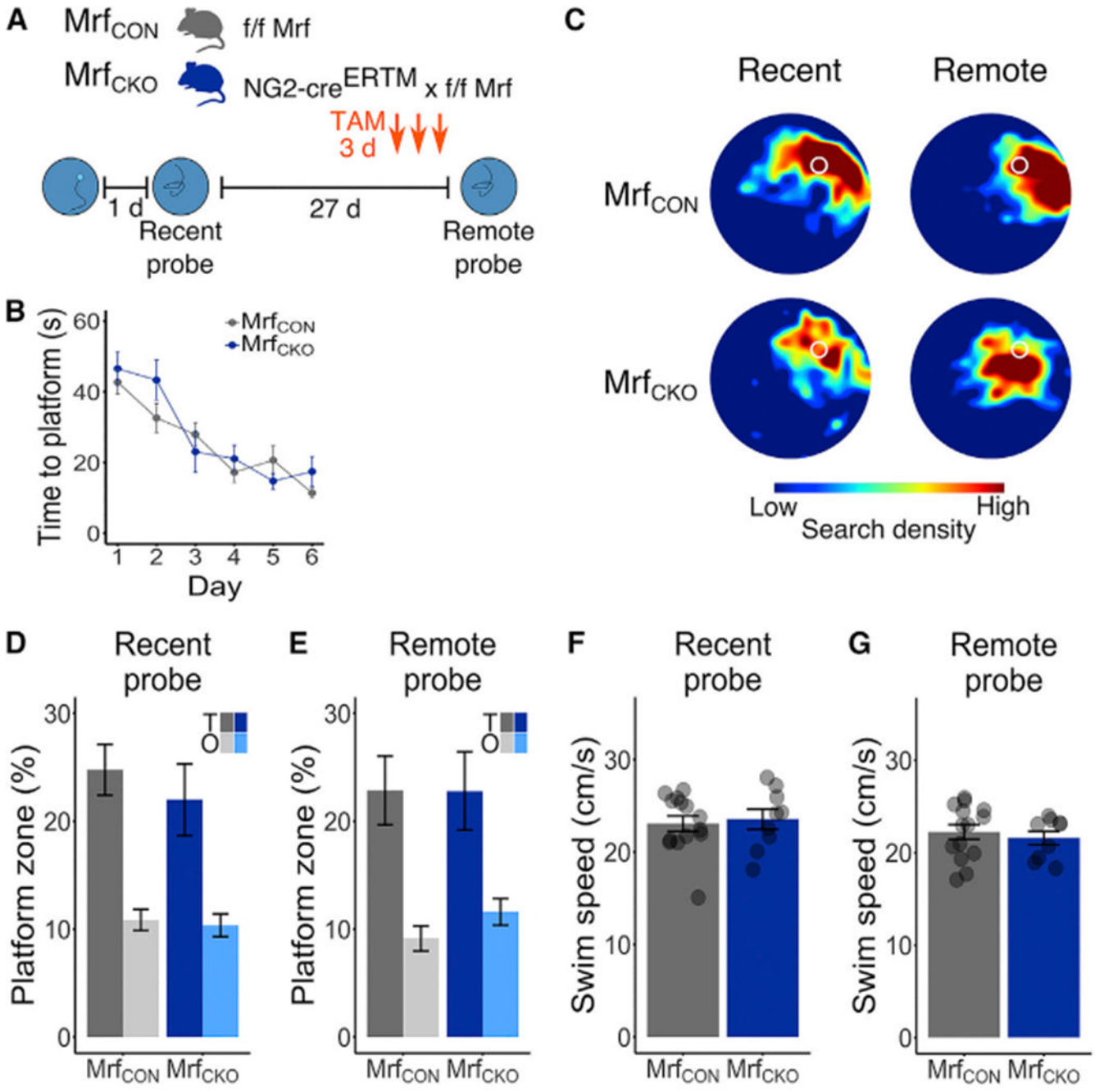

Figure 6. Delayed Disruption of Oligodendrogenesis Has No Effect on Spatial Memory Consolidation

(A) Experimental design. Mrf$_{CON}$ and Mrf$_{CKO}$ mice were trained in the water maze, and spatial memory was assessed in probe tests 1 day and 28 days later. Mice were treated with TAM 25 days after training to delete Mrf in OPCs before memory retrieval.

(B) During training, Mrf$_{CON}$ (n = 14) and Mrf$_{CKO}$ (n = 9) mice required progressively less time to locate the platform.

(C) Density plots illustrating probe test performance in recent and remote probe tests.

(D) In the recent probe test, both Mrf_{CON} and Mrf_{CKO} mice searched selectively, spending more time in the T zone versus O equivalent zones.
(E) In the remote probe test, both Mrf_{CON} and Mrf_{CKO} mice searched selectively, spending more time in the T zone versus O equivalent zones.(F and G) Swim speed was equivalent in Mrf_{CON} and Mrf_{CKO} mice during (F) the recent and (G) remote probe tests.
See also Figure S6. Pooled data are represented as mean ± SEM.

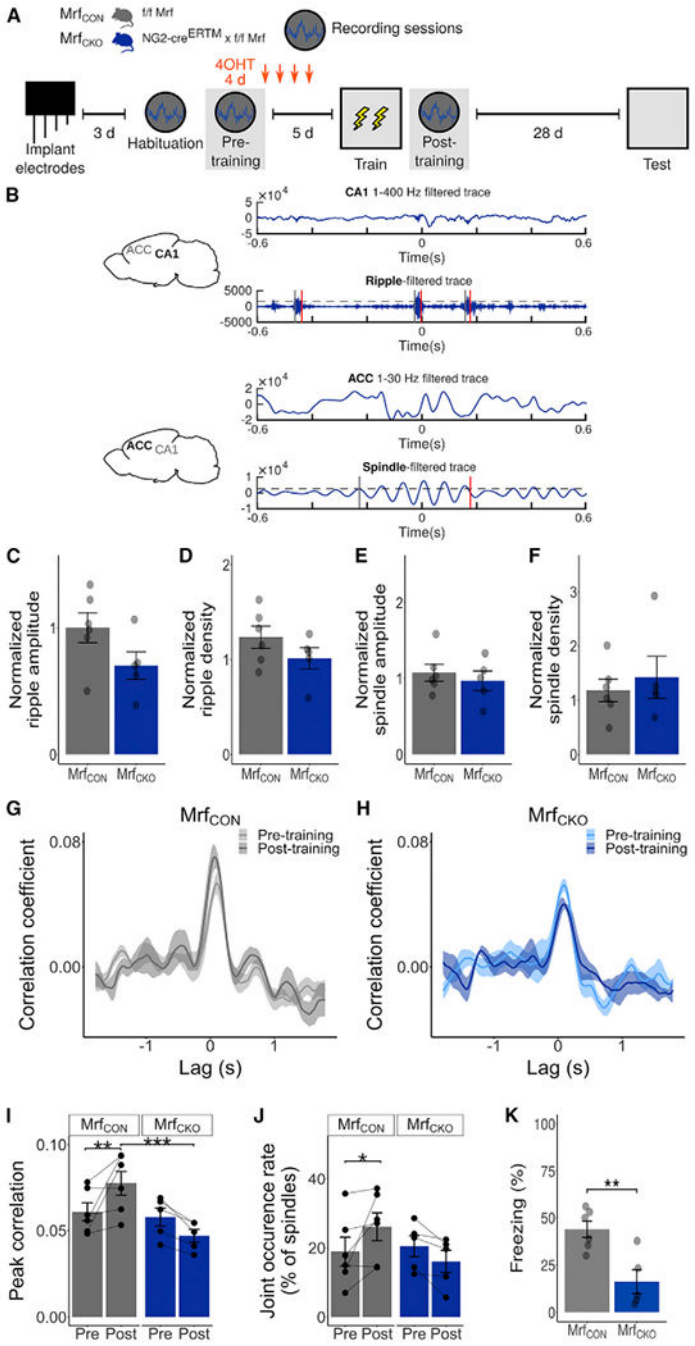

Figure 7. Disruption of Oligodendrogenesis Blocks a Learning-Induced Increase in Ripple-Spindle Coupling and Memory Consolidation

(A) Experimental design. Local field potential (LFP) electrodes were implanted in the ACC and CA1 region ofthe hippocampus in Mrf_{CON} (n = 6) and Mrf_{CKO} (n = 5) mice. Pre-training recordings of neural activity were acquired, and then mice were treated with 4OHT and contextual fear conditioned. Immediately after training, neural activity was recorded, and memory was tested 28 days later.

(B) Exampletraces of LFPs recorded inthe CA1 (top two traces, low-pass-filtered and ripple-band-filtered) and ACC (bottom twotraces, low-pass-filtered and spindle-band-filtered)

during a typical recording session in one mouse. Grey and red lines indicate detected ripple and spindle onset/offset, respectively.

(C and D) Relative to baseline, Mrf deletion in OPCs did not alter ripple amplitude (C) or density (D) (during the post-training session).

(E and F) Relative to baseline, Mrf deletion in OPCs did not alter spindle amplitude (E) or density (F) (during the post-training session).

(G and H) Instantaneous cross-correlation of ripple and spindle amplitude increased after learning in Mrf_{CON} mice (G), and Mrf deletion blocked this learning-induced increase in ripple-spindle coupling in Mrf_{CKO} mice (H).

(I) The peak of instantaneous cross-correlation for ripple-spindle coupling increased after learning in Mrf_{CON} mice, but Mrf deletion prevented this in Mrf_{CKO} mice.

(J) The joint occurrence rate, a second measure of coupling, increased in Mrf_{CON} mice after learning, and Mrf deletion prevent this increase in Mrf_{CKO} mice.

(K) In addition to preventing the learning-induced increase in neural coupling, blocking oligodendrogenesis impaired memory consolidation; Mrf_{CKO} mice displayed reduced freezing relative to Mrf_{CON} mice at the 28-day test.

See also Figure S7. Pooled data are represented as mean ± SEM.

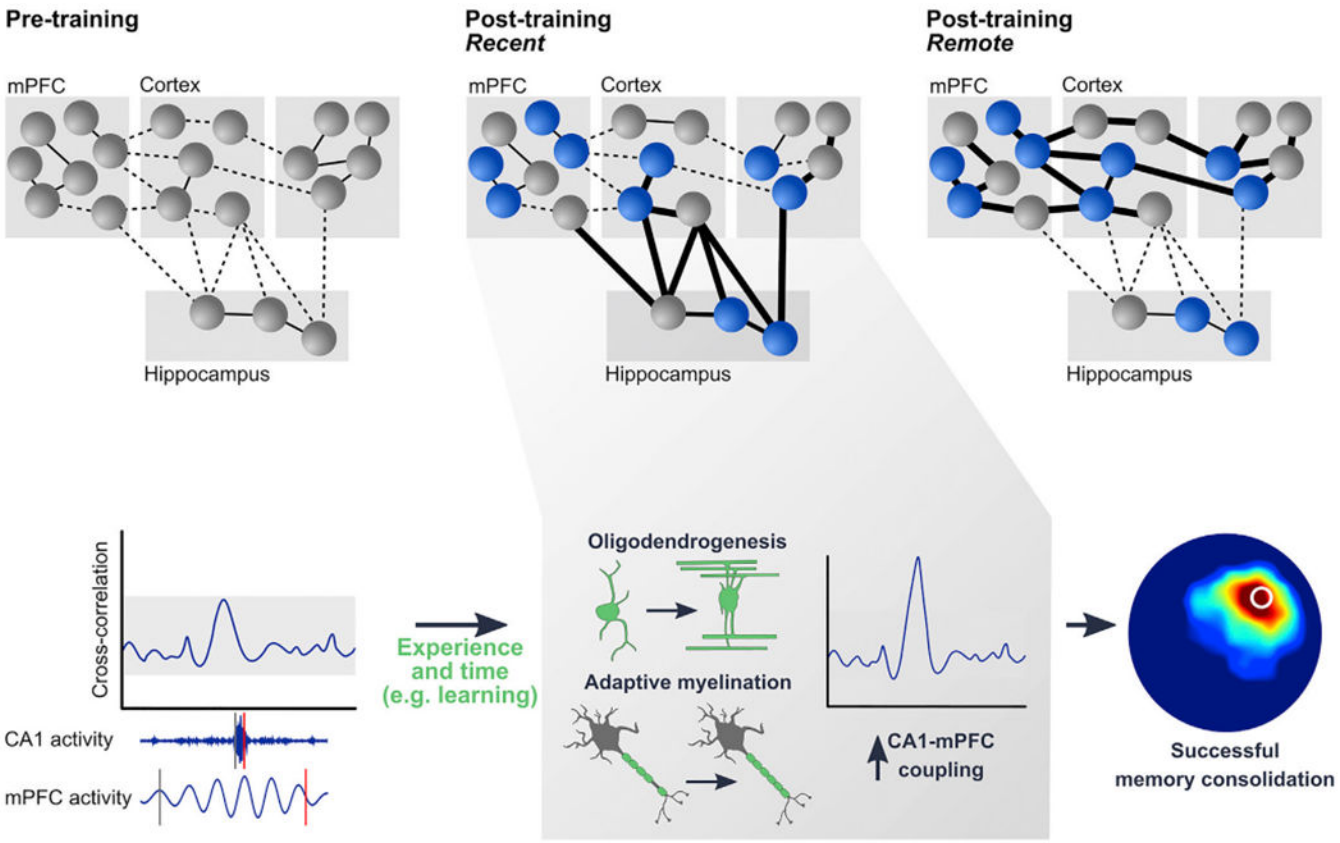

Figure 8. A Model Illustrating How Experience-Dependent Oligodendrogenesis Coordinates Neuronal Activity and Contributes to Memory Consolidation

After learning, coordinated reactivation of neural patterns in hippocampal-cortical circuits contribute toward the gradual consolidation and reorganization of memories (top). Oligodendrogenesis and *de novo* myelination facilitate learning-associated increases in hippocampal-cortical circuit synchrony (bottom). Therefore, oligodendrogenesis contributes to the circuit remodeling necessary for successful memory consolidation.

KEY RESOURCES TABLE

REAGENT or RESOURCE	SOURCE	IDENTIFIER
Antibodies		
Goat anti-PDGFRα	R & D Systems	Cat# AF1062
		RRID:AB_2236897
Mouse anti-CC1	Calbiochem (Millipore)	Cat# OP80
		RRID:AB_2057371
Rabbit anti-Olig2	Millipore	Cat# AB9610
		RRID:AB_570666
Mouse anti-NeuN	Millipore	Cat# MAB377
		RRID:AB_2298772
Rabbit anti-GFAP	DAKO	Cat# Z0334
		RRID:AB_10013382
Alexa 488 donkey anti-mouse	ThermoFisher Scientific	Cat# A-21202
		RRID:AB_141607
Alexa 647 donkey anti-rabbit	ThermoFisher Scientific	Cat# A-31573
		RRID:AB_2536183
Alexa 488 donkey anti-goat	ThermoFisher Scientific	Cat# A-11055
		RRID:AB_2534102
Alexa 488 donkey anti-rabbit	ThermoFisher Scientific	Cat# A-21206
		RRID:AB_2535792
Alexa 647 donkey anti-goat	ThermoFisher Scientific	Cat# A-21447
		RRID:AB_141844
Chemicals, Peptides, and Recombinant Proteins		
4-Hydroxytamoxifen	Toronto Research Chemicals	CAS: 68047-06-3
Tamoxifen	Toronto Research Chemicals	CAS: 10540-29-1
Normal Donkey Serum	Jackson ImmunoResearch	Code: 017-000-121
4’6’-diamidino-2-phenylindole (DAPI)	Sigma	CAS: 28718-90-3
Paraformaldehyde	Bioshop	CAS: 30525-89-4
Sodium Chloride	Bioshop	CAS: 7647-145
Potassium Chloride	Bioshop	CAS: 7447-40-7
Potassium Phosphate	Bioshop	CAS: 7778-77-0
Sodium Phosphate	Bioshop	CAS: 7558-79-4
Cremaphore	Sigma	CAS: 61791-12-6
Sunflower Seed Oil	Sigma	CAS: 8001-21-6
Anhydrous Alcohol	Sigma	CAS: 64-17-5
5-ethynyl-2′-deoxyuridine (EdU)	Carbosynth	CAS: 61135-33-9
Sulfo-cyanine3-azide	Lumiprobe	Cat# C1330
Copper (II) Sulfate ($CuSO_4$-$5H_2O$)	Sigma	CAS: 7758-99-8

REAGENT or RESOURCE	SOURCE	IDENTIFIER
L-Ascorbic Acid	Sigma	CAS: 50-81-7
Tris-base	Sigma	CAS: 77-86-1
Deposited Data		
Raw and analyzed data	This paper	https://data.mendeley.com/datasets/sy26r6ny66/
Experimental Models: Organisms/Strains		
Mouse: C57BL/6N	Taconic Bioscience	B6NTac
		RRID:SCR_016410
Mouse: NG2-cre^{ERTM}	The Jackson laboratory	RRID:IMSR_JAX:008538
Mouse: PDGFRα-cre^{ERTM}	The Jackson laboratory	RRID:IMSR_JAX:018280
Mouse: B6;129-*Myrf*^{tm1Barr}/J	The Jackson laboratory	RRID:IMSR_JAX:010607
Mouse: B6.129X1-Gt(ROSA)26Sor$^{tm1(EyFP)Cos}$/J	The Jackson laboratory	RRID:IMSR_JAX:006148
Mouse: Ai14 B6.Cg-Gt(ROSA)26Sor$^{tm14(CAG-tdTomato)Hze}$/J	The Jackson laboratory	RRID:IMSR_JAX:007914
Software and Algorithms		
WaterMaze	Actimetrics	https://www.actimetrics.com/products/watermaze/
Fiji v2.0.0-rc-68/1.52i (ImageJ)	ImageJ	https://fiji.sc
R v3.5.1 (2018-07-02)	R-project	https://www.r-project.org/
Inkscape (0.92)	Inkscape	https://inkscape.org/
MATLAB (R2017a)	The MathWorks	https://www.mathworks.com/products/matlab.html